# SEMMELWEIS EGYETEM DOKTORI ISKOLA

Ph.D. értekezések

3291.

### **BAJTAI ESZTER**

Molekuláris és experimentális onkológia című program

Programvezető: Dr. Bödör Csaba, egyetemi tanár

Témavezetők: Dr. Tóvári József, osztályvezető és

Dr. Füredi András, tudományos munkatárs

# CHARACTERIZATION OF THERAPY-INDUCED SENESCENCE IN BREAST CANCER: A REVERSIBLE AND DRUG-RESISTANT STATE

#### Ph.D. thesis

## Eszter Bajtai

# Doctoral School of Pathological Sciences Semmelweis University





Supervisors: József Tóvári, D.Sc.

András Füredi, Ph.D.

Official reviewers: Rita Padányi, Ph.D.

Tibor Pankotai, Ph.D.

Head of the Complex Examination Committee: Janina Kulka MD, D.Sc.

Members of the Complex Examination Committee: Zsuzsa Erdei, Ph.D.

Tamás Garay, Ph.D.

Budapest 2025

#### **Table of Contents**

L	ist of Abbreviations	5
1.	Introduction	9
	1.1. Cancer statistics: A threat not slowing down	9
	1.2. Mechanisms of drug resistance	9
	1.3. Cellular senescence: A state between life and death	11
	1.4. Many faces of cellular senescence	13
	1.5. How to identify senescent cells?	13
	1.5.1. Morphological and molecular changes	13
	1.5.2. Senescence-associated β-galactosidase	14
	1.5.3. Senescence-associated secretory phenotype (SASP)	14
	1.6. Senotherapeutics	15
	1.7. Emerging evidence on senescence escape	16
2.	Objectives	17
3.	Methods	18
	3.1. Cell lines and culture conditions	18
	3.2. Drugs	18
	3.3. TIS induction	18
	3.4. SA-β-Gal staining	19
	3.5. Drug treatment and viability assays	19
	3.6. Immunocytochemistry and fluorescent staining	20
	3.6.1. Immunocytochemistry	20
	3.6.2. Fluorescent staining	20
	3.7. Crystal violet staining	21
	3.8. Western Blotting	21
	3.9. Statistical analysis of <i>in vitro</i> experiments	21
	3.10. In vivo experiments	22
	3.11. RNA isolation and transcriptome analysis	22
	3.12. Single-cell RNA sequencing	23
	3.13. Cytokine Expression Assay	
	3.14. Surface and secreted proteins/peptides characterization	
	3.15. Mass spectrometry	26

4. Results	28
4.1. Assay development for the analysis of therapy-induced senescence	28
4.2. TIS induction and cellular characterization	29
4.3. Drug resistance and sensitivity profile of TIS breast cancer cells	31
4.4. Investigation of the response of TIS cells to senolytic treatments	36
4.4.1. Response to the senolytic agent Navitoclax	36
4.4.2. Response to additional senolytic compounds	38
4.5. Bulk RNA sequencing analysis of TIS	40
4.5.1. Pathway analysis	42
4.5.2. Drug resistance analysis	43
4.6. Single-cell RNA sequencing analysis of TIS	45
4.6.1. Clustering analysis of cell states	45
4.6.2. Investigation of senescence-associated transcriptional changes	47
4.6.3. Pathway analysis	48
4.6.4. Trajectory analysis of cell states	49
4.6.5. Drug resistance analysis	50
4.7. Investigation of the immunomodulatory effect of TIS cells	51
4.8. Surface proteomic profiling of TIS	52
5. Discussion	55
6. Conclusions	59
7. Summary	60
8. References	61
9. Bibliography of the candidate's publications	76
10. Acknowledgements	

#### **List of Abbreviations**

ABCB - ATP Binding Cassette Subfamily B

ACSM2A - Acyl-CoA Synthetase Medium Chain Family Member 2A

ANXA2 - Annexin A2

BIRC3 - Baculoviral IAP Repeat Containing 3

BRCA1 - Breast Cancer gene 1

BSA - bovine serum albumin

BTK - Bruton tyrosine kinase

bulk RNA-seq - bulk RNA sequencing

CA10 - Carbonic Anhydrase 10

CCL - C-C motif ligand

CDK - Cyclin-dependent kinase

CDKN1A - Cyclin Dependent Kinase Inhibitor 1A

CLEC - C-Type Lectin Domain Family

COL4A3 - Collagen type IV alpha 3 chain

CTR - Control

CXCL - (C-X-C motif) ligand

CYP - Cytochrome P450

DAMP - Damage-Associated Molecular Patterns

DCK - Deoxycytidine Kinase

DEGs - Differentially expressed genes

DNMT - DNA Methyltransferase 1

DOX - Doxorubicin

DOXIL - Pegylated liposomal doxorubicin

DTP - Drug-tolerant persister

EGFR - Epidermal Growth Factor Receptor

ENO1 - Enolase 1

FBL - Fibrillarin

FGFR1 - Fibroblast Growth Factor Receptor 1

FLNA - Filamin A

FLT3 - Fms Related Receptor Tyrosine Kinase 3

GDF15 - Growth Differentiation Factor 15

GRID2 - Glutamate Ionotropic Receptor Delta Type Subunit 2

GSDMC - Gasdermin C

GSEA - Gene Set Enrichment Analysis

HDAC - Histone deacetylase

HMGB1 - High Mobility Group Box 1

IDH2 - Isocitrate Dehydrogenase (NADP(+)) 2

IFIT - Interferon Induced Protein With Tetratricopeptide Repeats

IFITM - Interferon Induced Transmembrane Protein

IL - Interleukin

KRT6A - Keratin 6A

LGALS9 - Galectin 9

LMNB1 - Lamin B1

MACC - MET Transcriptional Regulator

MAPK - Mitogen-activated protein kinase

MKI67 - Marker Of Proliferation Ki-67

MMP - Matrix metalloproteinases

MSigDB - Molecular Signatures Database

mTOR - Mammalian target of rapamycin

NEDD8 - NEDD8 Ubiquitin Like Modifier

NES - Normalized enrichment scores

NF-κB - Nuclear factor kappa B

NK cell - Natural killer cells

NME2 - NME/NM23 Nucleoside Diphosphate Kinase 2

NTRK2 - Neurotrophic receptor tyrosine kinase 2

OIS - Oncogene-induced senescence

PARP1 - Poly(ADP-Ribose) Polymerase 1

PBS - Phosphate-buffered saline

PDE1A - Phosphodiesterase 1A

PDGF-AA - Platelet-Derived Growth Factor AA

PFA - paraformaldehyde

PI3K - Phosphoinositide 3-kinase

PLK1 - Polo Like Kinase 1

PSM - Proteasome 20S Subunit

PVDF - Polyvinylidene difluoride

**REPOP** - Repopulation

re-TIS - Re-therapy-induced senescence

RRM1 - Ribonucleotide Reductase Catalytic Subunit M1

SAMHD1 - SAM And HD Domain Containing Deoxynucleoside Triphosphate

Triphosphohydrolase 1

SA-β-Gal - Senescence-associated β-galactosidase

SASP - Senescence-associated secretory phenotype

scRNA-seq - single-cell RNA sequencing

SDS-PAGE - sodium dodecyl sulfate-polyacrylamide gel electrophoresis

SRSF - Serine And Arginine Rich Splicing Factor

 $TGF-\beta$  - Transforming growth factor-beta

TIS - Therapy-induced senescence

TNBC - Triple-negative breast cancer

TOP2A - DNA Topoisomerase II Alpha

TREM1 - Triggering Receptor Expressed On Myeloid Cells 1

UMAP - Uniform Manifold Approximation and Projection

VEGF - Vascular endothelial growth factor

XPO1 - Exportin 1

#### 1. Introduction

#### 1.1. Cancer statistics: A threat not slowing down

The growing number of individuals living with cancer underscores its continued significance in global health care. In 2022 alone, nearly 20 million new cancer cases were diagnosed, over 9.7 million cancer-related deaths were reported, and more than 53 million people were living with cancer within five years of their diagnosis (1). Breast cancer is the most frequently diagnosed cancer in women, representing 23.8% of all newly identified female malignancies. Each year, over 2.3 million women are diagnosed, and more than 8.1 million are living with the disease within five years of their initial diagnosis. In Hungary, breast cancer is the most frequently diagnosed cancer in women and the third most common malignancy overall, with over 7600 new cases and more than 30.000 five-year prevalent cases reported in 2022 (1). Despite advances in therapy, recurrence and drug resistance remain major clinical challenges. Tumors may initially respond well, but resistance often emerges over time, reducing treatment efficacy and limiting long-term survival (2).

#### 1.2. Mechanisms of drug resistance

Drug resistance remains one of the main challenges in oncology, contributing to the majority of treatment failures (3, 4). Malignant cells can evade therapeutic effects through several adaptive strategies (Figure 1), including the enzymatic inactivation of anticancer drugs or active removal from the intracellular environment (5, 6). Additionally, tumors may enhance their ability to repair treatment-induced DNA damage by increasing the activity of DNA repair pathways (7), or develop resistance by decreasing the availability of therapeutic targets at the protein level (8). Changes in survival-related signaling pathways can also make treatments less effective (9), or transient cell cycle arrest may help cancer cells avoid drugs that specifically target rapidly dividing cells (10). Each of these mechanisms is discussed in detail below, along with relevant examples.

One key pathway in drug resistance by drug inactivation involves cytochrome P450 enzymes, such as CYP3A4 and CYP3A5, which are capable of metabolizing and inactivating a wide range of chemotherapeutic drugs. For example in pancreatic tumor models, both *in vitro* and *in vivo*, tyrosine kinase inhibitor (TKI) therapies were found to be ineffective as long as CYP3A5 remained active (5).

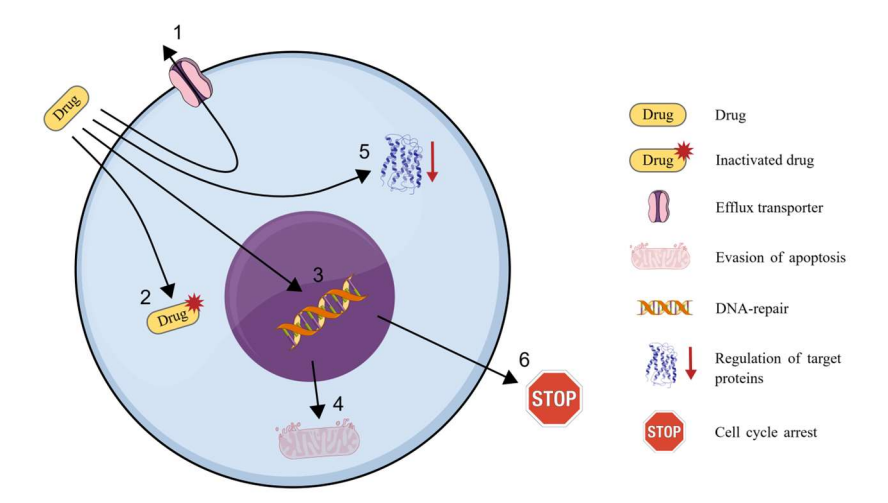


Figure 1. The most common mechanisms of drug resistance in tumor cells. These include: (1) drug efflux, (2) metabolic inactivation of therapeutic agents, (3) enhanced DNA damage repair, (4) evasion of apoptosis, (5) downregulation of drug targets, and (6) alterations in cell cycle regulation. This figure is adapted from Vajda et al. (11).

Another major contributor to drug elimination mechanisms is P-glycoprotein (ABCB1/Pgp), a member of the ATP-binding cassette (ABC) transporter family, which mediates drug efflux. This transporter uses energy from ATP hydrolysis to actively export compounds from the cell, thereby reducing intracellular drug concentrations and limiting treatment efficacy (6).

Most chemotherapeutics drugs induce significant DNA damage, to which tumor cells often respond by upregulating key DNA repair proteins such as BRCA1, BRCA2, and PARP1 (12).

Apoptosis can be avoided through the dysregulation of apoptotic signaling pathways. One example is chronic myeloid leukemia, where treatment with imatinib – a drug that induces apoptosis via a Bcl-2–dependent pathway in Bcr/Abl-positive leukemia cells – can become ineffective when tumor cells increase the expression of the anti-apoptotic protein Bcl-2, thereby blocking the cell death process (9).

Reduced expression of targets, such as topoisomerases I and II, leads to resistance to their inhibitors (13). Furthermore, the efficacy of many drugs depends on cell cycle phase – e.g., paclitaxel is only effective in M phase, not in G1 or G2 arrest (10, 14).

#### 1.3. Cellular senescence: A state between life and death

When cells experience DNA damage, their response depends on how severe the injury is. If the damage is relatively minor, the cell can typically initiate repair to regain normal function. In contrast, when the damage is too extensive to repair, the cell may undergo programmed death, such as apoptosis, or die uncontrollably through necrosis (15). However, between these two there is an intermediate response – cellular senescence – where cells remain viable but irreversibly exit the cell cycle.

The term "senescence" originates from the Latin word senex, meaning "old," and is commonly used to describe cellular states linked to aging. Cellular senescence was first identified by Hayflick and Moorhead in the 1960s, when they observed that normal human fibroblasts lose their ability to divide after a limited number of cell divisions – a phenomenon now known as the Hayflick limit. This state of permanent growth arrest, later termed replicative senescence, became a foundational concept in aging and cancer biology (16). Senescence has since been recognized as a protective response that limits the proliferation of damaged cells. Importantly, even though these cells can no longer divide, they remain metabolically active and affect their microenvironment through the secretion of various signaling molecules (17).

This activity has been linked to several beneficial processes. Senescent cells promote wound healing by secreting factors such as PDGF-AA, which stimulate the differentiation of fibroblasts and myofibroblasts, thereby accelerating tissue repair (18). Cellular senescence has also been identified as an important process during embryonic development. In embryogenesis, cells with senescence-associated features are present in both mouse and human embryos (19, 20). Additionally, Kang et al. demonstrated that premalignant senescent hepatocytes, through the secretion of chemokines and cytokines, can trigger an antigen-specific immune response – termed "senescence surveillance" – which is critical for suppressing tumor development in the liver (21). Moreover, senescent cells can induce senescence in neighboring cells via paracrine signaling, thereby reinforcing their tumor-suppressive role by preventing further proliferation (22, 23).

However, studies have shown that senescent cells can have several detrimental effects, such as their contribution to aging. A direct connection has been demonstrated between telomere shortening, cellular senescence, and organismal aging (24). For example, studies have shown that the number of senescent cells increases significantly with age in mice,

with elevated levels observed in organs such as the liver, skin, lungs, and spleen (25). Today, cellular senescence is widely recognized as one of the hallmarks of aging. While senescence may serve a beneficial role by limiting the proliferation of damaged cells, its accumulation can contribute to tissue dysfunction, chronic inflammation and tumor progression as well (26). Many studies showed that through the secretion of various factors, - known as the senescence-assotiated secretory phenotype (SASP) - senescent cells can negatively modulate the immune system, thereby contributing to cancer progression and relapse (27, 28). Ruhland et. al. showed that IL6-secreting senescent cells within the tumor stroma promote a pro-tumorigenic environment by recruiting immunosuppressive myeloid-derived suppressor cells, which inhibit cytotoxic T-cell responses and establish a chronic inflammatory microenvironment that facilitates early tumor growth (29). Another study demonstrated that CCL2 chemokines secreted by senescent hepatocytes recruit CCR2<sup>+</sup> immature myeloid cells, which initially contribute to senescent cell clearance but later suppress NK cell activity, thereby blocking tumor immune surveillance (30). SASP components have also been linked to angiogenesis, invasion, and metastasis. IL6, in particular, has been shown to support blood vessel formation (27), while other SASP signals can drive epithelial-to-mesenchymal transition (EMT) (31). Additionally, SASP activity may contribute to the reprogramming and dedifferentiation of nearby cells, potentially giving rise to cancer stem cell-like phenotypes (32).

Because of its complex role, cellular senescence is often described as a double-edged sword, contributing to both beneficial and harmful effects on surrounding tissues, depending on the physiological or pathological context (Figure 2).

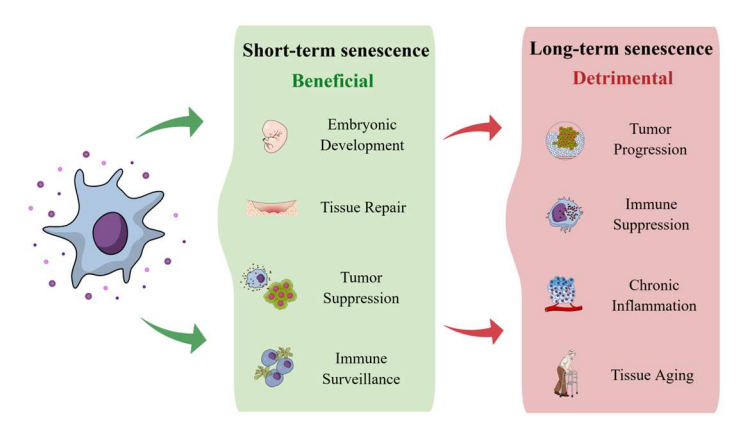


**Figure 2.** Dual role of cellular senescence. Transient senescence contributes to beneficial biological processes, while persistent senescence is associated with detrimental effects.

#### 1.4. Many faces of cellular senescence

Cellular senescence can be classified into two main types based on the initiating trigger: replicative senescence and stress-induced senescence. Replicative senescence results from telomere shortening after repeated cell divisions. In contrast, stress-induced senescence occurs in response to various internal and external stressors, such as oncogene activation (oncogene-induced senescence, OIS), cancer therapy (therapy-induced senescence, TIS), ionizing or UV radiation, and oxidative stress (33, 34).

OIS is a well-characterized cellular response that acts as a barrier to tumor development by halting cell proliferation following oncogenic activation. The initial discovery showed that the expression of mutant HRas<sup>G12V</sup> in human diploid fibroblasts induce cellular senescence through the activation of the p53 and p16<sup>INK4a</sup> pathways (35).

TIS can be induced by several chemotherapeutic drugs, such as doxorubicin, etoposide, and cisplatin, both *in vitro* and *in vivo* (36-38). Later, evidence from clinical samples has revealed elevated levels of senescence markers – such as SA-β-gal, p21, p16 – following neoadjuvant chemotherapy in patients with breast and prostate cancer (38, 39). Traditionally, TIS has been considered a beneficial outcome of cancer treatment, as it stops tumor cells from proliferating without necessarily causing cell death (40). However, increasing evidence suggests that TIS is not always a stable endpoint; some cells can escape this state over time (41, 42). These findings raise the possibility that TIS may contribute to therapy resistance and tumor relapse.

#### 1.5. How to identify senescent cells?

Identification is essential for investigating cellular senescence, yet remains challenging due to the broad and variable nature of the phenotype. While many markers have been established through *in vitro* studies, no single marker is sufficient on its own. Instead, combining multiple markers is considered a more reliable approach for detecting senescence (43, 44). Moreover, even using a combination of various markers, differentiating one type of senescence from another is nigh impossible. This section highlights the key markers commonly used to identify senescent cells.

#### 1.5.1. Morphological and molecular changes

The altered morphology of senescent cells was first described by Hayflick and Moorhead, who observed that cells undergoing replicative senescence appeared enlarged and

flattened, often accompanied by an increased nuclear size (45). Later, the enlarged nucleus has been linked to structural changes in the nuclear envelope, most notably the loss of Lamin B1, which is frequently used as a marker of senescence (46). Another characteristic of senescent cells is their stable arrest in the cell cycle. This arrest is typically enforced by the upregulation of key regulatory proteins, including p16, p21, p27, and p53 (47). At the same time, senescent cells show reduced expression of proliferation-associated markers such as Ki67 (48).

#### 1.5.2. Senescence-associated β-galactosidase

Senescence-associated  $\beta$ -galactosidase (SA- $\beta$ -Gal) is one of the most commonly used markers to detect senescent cells both *in vitro* and *in vivo*. This marker reflects increased lysosomal content, a characteristic feature of senescent cells. While  $\beta$ -galactosidase normally functions at an acidic pH of around 4.5, in senescent cells the enzyme remains active at pH 6.0, allowing its detection through histochemical staining (49). First described by Dimri et al. in 1995, SA- $\beta$ -Gal positivity has since been widely applied in aging and cancer research. However, its use has limitations, as  $\beta$ -galactosidase activity can also be detected in certain non-senescent contexts, such as in cells undergoing contact inhibition or starvation (50).

#### 1.5.3. Senescence-associated secretory phenotype (SASP)

A hallmark of senescent cells is their secretory behavior, commonly referred to as the SASP. This complex profile includes a wide range of cytokines, chemokines, proteases, and growth factors, which vary depending on the cell type and the senescence-inducing stimulus. Commonly assessed SASP components include interleukins (e.g., IL6, IL8), chemokines (e.g., CCL2, CXCL1), extracellular matrix-modifying enzymes (e.g., MMP-1, MMP-9), and growth factors such as VEGF and TGF-β (17). While the SASP can contribute to beneficial processes like immune clearance of senescent cells and tissue repair, it can also promote chronic inflammation and tumor progression (17, 18, 51, 52). Although SASP profiling is widely used to detect senescent cells, its heterogeneity limits its reliability as a universal biomarker. Therefore, SASP components should be selected carefully based on the experimental context and used in combination with other senescence markers for accurate identification.

The most commonly used senescence markers, along with their associated molecular features and detection methods are summarized in Table 1.

**Table 1.** The most commonly used senescence markers and their detection methods (53).

Cellular Senescence Hallmark	Biomarker	Expected change	Detection
Morphological changes	Size, morphology	Enlarged, flattened	Light microscopy
Lysosomal activity	SA-β-galactosidase	increased	Staining
DNA damage	γH2AX	increased	IF
Cell cycle arrest	p21, p53, p16INK4a, pRB	increased	WB, IF
Nuclear membrane	Lamin B1	decreased	WB, IF, qPCR
SASP	Cytokine secretion	increased	ELISA, WB

#### 1.6. Senotherapeutics

To counteract the negative effects caused by the presence of senescent cells, senotherapy approaches have been developed. These are separated into two main categories: senolytics, which selectively eliminate senescent cells, and senomorphics, which suppress their harmful secretory phenotype (SASP) without inducing cell death (54). In general, senomorphic agents suppress SASP expression by targeting key signaling pathways such as NF-κB, mTOR, IL-1α, and p38 MAPK (54). For instance, rapamycin, a wellcharacterized senomorphic compound, inhibits the mTOR pathway, thereby reducing the secretion of SASP-associated inflammatory cytokines (55). The first senolytic agents were identified by Zhu et al., who demonstrated that the combination of the tyrosine kinase inhibitor dasatinib and the flavonoid quercetin effectively eliminated senescent cells (56). Subsequently, other plant-derived compounds, such as piperlongumine and fisetin, also showed senolytic activity (57, 58). The largest group of senolytic agents targets anti-apoptotic Bcl-2 family proteins, including Bcl-2 and Bcl-xL, which are commonly upregulated in senescent cells to support their survival. Inhibitors such as navitoclax (ABT-263), ABT-737, and A-1331852 have demonstrated selective senolytic effects through this mechanism (59-61). Although senotherapeutics show great promise in extending healthspan and treating age-related diseases, their clinical translation remains challenging due to off-target effects. For example, rapamycin treatment has been associated with insulin resistance, while the elimination of senescent cells can impair tissue repair and delay wound healing, underscoring the need for more selective and safer therapeutic strategies (18, 62).

#### 1.7. Emerging evidence on senescence escape

In recent years, increasing evidence has questioned the long-standing view of senescence as a stable, irreversible growth arrest. Traditionally, senescence has been seen as a favorable outcome of cancer therapy, especially when complete elimination of tumor cells cannot be achieved, as it halts cell proliferation and limits disease progression (40). However, a growing number of studies now suggest senescent cells can escape this arrested state.

In the early years, Robertson et al. demonstrated that a small subset of p53- and p16-deficient non-small cell lung cancer cells was able to escape therapy-induced senescence and re-enter the cell cycle, particularly in the presence of Cdc2/Cdk1 overexpression (41). Saleh et al. investigated the ability of TIS cells to escape growth arrest in several cancer cell lines, including H460, A549, and HCT116 BTG1-RFP, following treatment with different drugs. Their findings showed that, in the majority of cases, the senescent cells eventually resumed proliferation (42, 63). Milanovic et al. demonstrated that lymphoma cells escaping therapy-induced senescence upon p53 or Suv39h1 inactivation exhibit enhanced stemness and increased tumorigenic potential (64). Yang et al. reported a spontaneous reversion of A549 senescent cells to a proliferative state following Adriamycin exposure, without requiring p53 inactivation (65).

These findings collectively underscore the potential for TIS cells to regain proliferative capacity and actively contribute to relapse during cancer treatment.

#### 2. Objectives

In my PhD research, I set the following objectives:

- To characterize therapy-induced senescence (TIS) in a panel of breast cancer cell lines using multiple senescence-associated markers.
- To investigate the reversibility of TIS and the characteristics of repopulating (REPOP) cells.
- To profile the drug resistance and sensitivity landscape of TIS cells.
- To analyze transcriptomic and proteomic changes associated with TIS.
- To evaluate the response of TIS cells to senolytic treatments and test their therapeutic potential.

#### 3. Methods

#### 3.1. Cell lines and culture conditions

Human breast cancer cell lines (MCF7, T47D, MDA-MB-231, Hs578T) were acquired from the Developmental Therapeutics Program of the National Cancer Institute (NIH, Bethesda, MD, USA). Cells were maintained in Roswell Park Memorial Institute (RPMI) medium (Thermo Fisher Scientific, MA, USA) supplemented with 10% fetal bovine serum (FBS; Thermo Fisher Scientific), 5 mM L-glutamine (Euroclone, Pero MI, Italy), and 50 U/mL penicillin–streptomycin mixture (Capricorn Scientific, Ebsdorfergrund, Germany). Cultures were incubated at 37 °C and 5% CO<sub>2</sub>.

#### **3.2. Drugs**

The following drugs were used during this study.

(R)-MG132, 4-Methylsalicyclic acid, 5-Azacytidine, 5-fluoro-2'-deoxycytidine, Actinomycin D, Belinostat, Bortezomib, Dimethyl 2-oxoglutarate, Doxorubicin, Simvastatin, Thymoquinone (Merck Life Science, Darmstadt, Germany)

A-1331852, ABT-737, Amifostine, Chlormethine, Covidarabine, Cyclophosphamide, Dasatinib, Dexamethasone, Docetaxel, Fisetin, Gemcitabine, Glasdegib, Histamine, Ivosidenib, Laromustine, Lenalidomide, Meloxicam, Metformin, Methylprednisolone, Mitoxantrone, Navitoclax, Paclitaxel, Piperlongumine, Pixantrone, Plerixafor, Pracinostat, Pravastatin, Quercetin, Quizartinib, Ricolinostat, Romidepsin, Selinexor, Sorafenib, Sunitinib, Temozolomide, Thalidomide, Tipifarnib, Troxacitabine, Valproic acid, Venetoclax, Voreloxin, Vorinostat, Zosuquidar (MedChemExpress, New Jersey, USA)

AT-7519, Bisantrene, Carfilzomib, Chlorambucil, Cladribine, Clofarabine, Crenolanib, Cytarabine, Dinaciclib, Duvelisib, Enasidenib, Gefitinib, Gilteritinib, HDAC-42, Homoharringtonine, Ibrutinib, Idasanutlin, Ixazomib, Masitinib, Melphalan, Nintedanib, Panobinostat, Pevonedistat, SB-1317, Vincristine, Volasertib (Selleck Chemicals LLC, Houston, USA)

#### 3.3. TIS induction

TIS was induced by treating cells with doxorubicin (DOX) – 120 nM (MCF7), 70 nM (T47D), 150 nM (MDA-MB-231), and 200 nM (Hs578T) – for 5 days. Following the 5-

day treatment, the medium was removed, and cells were washed with PBS. Fresh medium was added to allow cells to recover. To confirm the onset of senescence, cultures were maintained under standard conditions (37 °C, 5% CO<sub>2</sub>) for an additional 7 days, allowing for the establishment of the senescent phenotype.

The concentrations applied were determined based on preliminary cytotoxicity dose-response experiments, in which 1 million cells were seeded per T75 flask and treated with a range of drug concentrations. The selected doses induced over 90% cell death over time, while still allowing repopulation.

To generate re-TIS cells, REPOP cells were replated and subjected to a second round of DOX treatment to re-induce senescence.

#### 3.4. SA-β-Gal staining

Cells were seeded into 96-well tissue culture plates and stained using the Senescence β-Galactosidase Staining Kit (Cell Signaling Technology, Danvers, MA, USA). Cells were fixed using a fixative solution, washed with PBS, and incubated overnight at 37 °C in X-gal staining solution under CO<sub>2</sub>-free conditions. On the following day, the staining solution was removed and replaced with 70% glycerol to prepare the samples for brightfield microscopy.

#### 3.5. Drug treatment and viability assays

To assess drug sensitivity, 10.000 cells per well were seeded into 96-well tissue culture plates. TIS was established as described in Section 3.3. Following TIS induction, the number of viable cells in three replicate wells was determined and averaged. An equivalent number of CTR cells was then plated to ensure comparable cell density for subsequent drug testing.

On the following day, both TIS and CTR cells were exposed to a concentration gradient of selected compounds and incubated for five days under standard conditions. Drug treatments were also applied to re-TIS cells under similar experimental conditions. To generate re-TIS cells, 10.000 REPOP cells per well were plated in 96-well plates and subjected to a second round of doxorubicin treatment for five days. After treatment, cells were gently washed with pre-warmed PBS and replenished with fresh culture medium. Cells were then maintained for seven additional days to allow for phenotypic

stabilization. On Day 12, the re-TIS cells were treated with the selected drug panel for comparative analysis.

Cell viability was assessed using the PrestoBlue<sup>TM</sup> Cell Viability Reagent (Thermo Fisher Scientific, MA, USA), following the manufacturer's instructions. Cells were incubated with 5% PrestoBlue<sup>TM</sup> diluted in PBS for 1.5 hours at 37 °C in 5% CO<sub>2</sub>. Fluorescence intensity was measured using an EnSpire microplate reader (PerkinElmer, Waltham, MA, USA). Viability values were normalized to untreated controls. Dose–response curves were generated using the nonlinear regression (sigmoidal dose-response) model in GraphPad Prism v8.0.1 for Windows (GraphPad Software, Boston, MA, USA).

#### 3.6. Immunocytochemistry and fluorescent staining

TIS and CTR cells were seeded onto glass-bottomed 8-well chamber slides (ibidi, Gräfelfing, Germany) at a density of 20.000 cells per well. Senescence induction was conducted as described in Section 3.3.

#### 3.6.1. Immunocytochemistry

Cells were fixed with 4% paraformaldehyde (PFA) for 15 minutes at room temperature, followed by two washes with PBS. Permeabilization and blocking were performed for 1 hour at room temperature using a solution containing 0.5% bovine serum albumin (BSA) in PBS, 0.1% Triton X-100, 5% goat serum, and 1% fish gelatin.

Primary antibodies against γ-H2A.X, Bcl-2, and Bcl-XL (Thermo Fisher Scientific, Waltham, MA, USA) were applied overnight at 4 °C. After incubation, cells were washed with PBS and incubated with Alexa Fluor 488-conjugated secondary antibody (Thermo Fisher Scientific, Waltham, MA, USA) diluted in blocking solution. Nuclear staining was carried out using DAPI (Dojindo EU, Munich, Germany). Imaging was performed with a Zeiss LSM-710 confocal microscope using a 40× objective.

#### 3.6.2. Fluorescent staining

The following dyes and detection kits were used according to the manufacturer's protocols (Dojindo EU, Munich, Germany): Nucleolus Bright Red, SPiDER-βGal Cellular Senescence Detection Kit, MitoBright Red, LysoTracker Red. All samples were imaged under a Zeiss LSM-710 confocal microscope at 40× magnification.

#### 3.7. Crystal violet staining

Cells were plated in 6-well plates at a density of 100.000 cells/ well. Following five days of doxorubicin treatment, cells were washed with pre-warmed PBS and fresh medium was added. The next day, treatment with navitoclax was initiated at the previously determined IC<sub>30</sub> concentration, and administered three times per week for a duration of two weeks. For staining, a stock solution of 0.5% (w/v) crystal violet (Merck, Darmstadt, Germany) was prepared in 25% methanol. A 10-fold diluted working solution was then prepared using the same methanol concentration. Cells were washed twice with PBS, and the plates were placed on ice. Fixation was carried out using ice-cold 100% methanol for 5-10 minutes. After fixation, 1 mL of the diluted crystal violet solution was added to each well and incubated at room temperature for 5-10 minutes. Excess stain was removed by washing the wells multiple times with distilled water. Plates were then air-dried overnight.

#### 3.8. Western Blotting

Cells were lysed using a buffer containing 50 mM HEPES (pH 7.3), 150 mM NaCl, 10% glycerol, 1% Triton X-100, 1 mM EDTA, and 1.5 mM MgCl<sub>2</sub>, supplemented with protease inhibitors. Samples were separated by SDS-PAGE then transferred to PVDF membrane (Bio-Rad, Hercules, California, USA). Membranes were probed overnight at 4°C with primary antibodies against CDKN1A (p21), LMNB1 (Cell Signaling Technology, Danvers, MA, USA), Bcl-2 (Thermo Fisher, Waltham, MA, USA), and Bcl-XL, ACSM2A, GSDMC, PSMA8, PDE1A (Proteintech, Rosemont, USA), followed by incubation with HRP-conjugated secondary antibodies. Signal detection was performed using an ECL chemiluminescent detection system (WesternBright ECL kit, Advansta, San Jose, USA) and a Chemidoc MP device (Bio-Rad, Hercules, California, USA). Band intensities were quantified by densitometry using Image Lab software (Bio-Rad, Hercules, California, USA).

#### 3.9. Statistical analysis of in vitro experiments

All experiments were performed with a minimum of three independent biological replicates. Statistical analyses were carried out using GraphPad Prism version 8.0.1 (GraphPad Software, Boston, MA, USA). Data were analyzed using either a one-way analysis of variance (ANOVA) or unpaired two-tailed Student's t-test, as appropriate. P-

values were interpreted according to the following thresholds:  $p \le 0.05$  (\*),  $p \le 0.01$  (\*\*),  $p \le 0.001$  (\*\*\*), and  $p \le 0.0001$  (\*\*\*\*). Differences with p > 0.05 were considered not statistically significant (n.s.).

#### 3.10. In vivo experiments

All animal studies were conducted in accordance with the European Union directives on the protection of animals used for scientific purposes, and were approved by the Hungarian Animal Health and Animal Welfare Directorate. Experimental protocols were performed according to the Committee on the Care and Use of Laboratory Animals of the Department of Experimental Pharmacology at the National Institute of Oncology (Budapest, Hungary) (Permit numbers: PEI/001/1738-3/2015 and PE/EA/1461-7/2020).

1 mm³ fragments of mammary tumors derived from Brca1-/-;p53-/- FVB mice (a

1 mm³ fragments of mammary tumors derived from Brca1-/-;p53-/- FVB mice (a generous gift from Sven Rottenberg, NKI) were implanted into the mammary fat pad of wild-type female FVB mice (Department of Experimental Pharmacology, National Institute of Oncology, Budapest, Hungary) under anesthesia (20 mg/kg zolazepam, 12.5 mg/kg xylazine, 3 mg/kg butorphanol, 20 mg/kg tiletamine). Tumor growth was monitored at least three times weekly using caliper measurements, starting from the time tumors became palpable. Tumor volumes were calculated using the standard formula: V = (length × width²)/2. When tumors reached approximately 200 mm³, treatment with DOXIL was initiated at the maximum tolerated dose (6 mg/kg, intravenous). Navitoclax treatment began two days later, administered for 10 days at 50 mg/kg. Mice were euthanized when tumors reached ~2000 mm³. Survival data were evaluated using Kaplan–Meier curves, and statistical differences between groups were assessed using the log-rank (Mantel–Cox) test.

#### 3.11. RNA isolation and transcriptome analysis

The bioinformatic processing and analysis of the bulk RNA-seq data were performed by Anna Lovrics.

MCF7, T47D, MDA-MB-231 and Hs578T TIS cells were harvested on Day 12. CTR and REPOP cells were harvested at ~80% confluency. Cells were homogenized in TRIzol<sup>TM</sup> Reagent (Thermo Fisher Scientific, Massachusetts, USA). Total RNA was extracted from samples using Direct-zol® MiniPrep kit (Zymo Research, Irvine, California, USA) following the manufacturer's instructions. To prevent DNA contamination, an in-column

DNAse I treatment was performed. The prepared total RNA samples were sent to Xenovea Ltd. (Szeged, Hungary) for transcriptome analysis. The RNA concentration was determined by using the Qubit RNA HS Assay Kit on the Qubit 3.0 Fluorometer (Thermo Fisher Scientific, Waltham, MA, USA). Quality CTR was assessed by Labchip GX Touch HT instrument on DNA 5K/RNA/CZE Chip (Perkin Elmer, Waltham, MA, USA) with RNA Pico Sensitivity Assay Reagents (Perkin Elmer, Waltham, MA, USA). NextFlex PolyA beads 2.0 kit and NextFlex Rapid Directional RNA-seq Kit 2.0 with UDIs (Perkin Elmer, Waltham, MA, USA) were used for mRNA capture and strand-specific library preparation. The library quantities were measured by Quant-iT 1x dsDNA HS Assay kit (Thermo Fisher, Waltham, MA, USA) with Fluostar Omega (BMG Labtech, Ortenberg, Germany). The fragment size distribution of the libraries was determined by capillary electrophoresis on Labchip GX Touch Nucleic Acid Analyzer on XMark HT chip by using DNA NGS 3k Assay kit (Perkin Elmer, Waltham, MA, USA). Pooled libraries were sequenced with 50M 150 bp paired-end reads on NovaSeq 6000 platform (Illumina, San Diego, CA, USA). A standard RNA sequencing pipeline was used for analysis: preprocessing with the Fastq Toolkit (v2.2.5), mapping reads by STAR (v2.7.10) and obtaining gene counts using Subread's (v2.0.3) Feature counts function. Next, limma (v3.58.1) and fgsea (v1.28.0) pipelines were applied to obtain differential gene expression and enriched gene sets respectively.

#### 3.12. Single-cell RNA sequencing

The bioinformatic processing and analysis of the single-cell RNA-seq data were performed by Csaba Kiss and Sándor Spisák.

MCF7 and T47D cells from CTR, TIS at day 12, and repopulating REPOP conditions were collected via trypsinization. For each sample, 15,000 cells were used. Two biological replicates of single-cell suspensions were prepared using Scipio Bioscience's RevGel-seq<sup>TM</sup> technology – a reversible hydrogel-based, instrument-free 3' scRNA-seq platform – in conjunction with the Asteria<sup>TM</sup> benchtop kit. This method enables uniform coupling of cells with solid polymer-barcoded beads in a homogeneous phase. Following cell capture, standard steps were performed including cell lysis, mRNA capture on barcoded beads, reverse transcription, PCR amplification, and cDNA sequencing. Sequencing was performed on a NovaSeq platform using 75 bp paired-end sequencing chemistry to yield approximately 35,000 raw reads per cell.

Read alignment to the Human Scipio 2022 A reference genome was carried out using the Cytonaut platform (v2.1.0). Output files (features.tsv.gz, barcodes.tsv.gz, and matrix.mtx.gz) were imported into R and processed using the Seurat package (v5.1.0). Doublets were identified and removed using DoubletFinder (v2.0.4). MCF7 and T47D datasets were then processed separately, with all cells per sample type merged into a single Seurat object. Further filtering excluded cells with >10% mitochondrial RNA content, >30,000 UMIs, <500 detected genes, or <1,000 UMIs. Standard Seurat workflows were followed: NormalizeData (LogNormalize method, scale factor = 10,000), identification of variable genes with FindVariableFeatures, scaling with ScaleData, and principal component analysis using RunPCA. Batch correction was not applied, as sample consistency was high and correction risked masking biological variation. For clustering, FindNeighbors was run using the first 15 principal components (PCs) for MCF7 and 20 PCs for T47D, followed by FindClusters (resolution = 0.3 for MCF7, 0.5 for T47D). UMAP embeddings were calculated with RunUMAP using the same respective PCs. Cell cycle stage inference was conducted with CellCycleScoring. Differential gene expression analysis was performed using FindMarkers, and gene set enrichment analysis (GSEA) was conducted using the clusterProfiler package (v4.6.2). For combined analysis, MCF7 and T47D datasets were merged into a single Seurat object and processed using the same pipeline, employing 15 PCs for both FindNeighbors and RunUMAP, and clustering at resolution 0.5. Trajectory inference was performed using Monocle3 (v1.3.1), focusing on the transitions CTR→TIS and TIS→REPOP for both cell lines. The top 200 trajectory-associated genes were identified and compared across cell lines and conditions, yielding 92 overlapping differentially expressed genes (DEGs), including CDKN1A. Pseudobulk TMM-FPKM values for these genes were calculated, Z-score normalized, and visualized via heatmap.

#### 3.13. Cytokine Expression Assay

The cytokine expression assay was carried out by Károly Hegedűs.

Total RNA was isolated from MCF7 and T47D parental (CTR) and senescent (TIS) cells using TRI Reagent® (Molecular Research Center, Cincinnati, OH), following the manufacturer's instructions. RNA was resuspended in 14 µL diethyl pyrocarbonate-treated water, and its concentration and purity were assessed using a NanoDrop 1000 spectrophotometer (Thermo Fisher Scientific, Waltham, MA). mRNA was reverse

transcribed using the Maxima First Strand cDNA Synthesis Kit (Thermo Fisher Scientific) according to the manufacturer's protocol. Cytokine mRNA expression was analyzed using the high-throughput BioMark HD real-time qPCR platform (Fluidigm, South San Francisco, CA) with the Flex Six<sup>TM</sup> Gene Expression IFC chip (Fluidigm). Before qPCR analysis, a 12-cycle cDNA preamplification step and an exonuclease treatment were performed, followed by a 10-fold dilution of the final product. Cytokine expression levels were quantified using SsoFast<sup>TM</sup> EvaGreen® Supermix with Low ROX (Bio-Rad Laboratories, Hercules, CA) and primers specific to cytokines and reference genes, according to the manufacturer's recommendations. The cytokine panel included IL6, IL10, IL13 while expression was normalized using four reference genes: G6PD, GAPDH, PPIB, and RPIIA. This cytokine expression assay was originally developed in our laboratory to assess immunosuppression efficiency in heart transplant patients receiving tacrolimus and methylprednisolone. Cytokine expression data were normalized to the average cycle threshold (Ct) of the four reference genes to ensure accurate quantification.

#### 3.14. Surface and secreted proteins/peptides characterization

The proteomic experiments and data analyses were carried out by Gábor Tusnády and Tamás Langó.

To identify the targetable proteome on the surface of the CTR, TIS and REPOP MCF7 cells, we used a high-throughput surface biotinylation method similarly as described in the previous works (66, 67). Parental and repopulated cells were cultured until they reached ~80% confluency before labeling, while TIS cells were processed on day 7 after doxorubicin removal. First, the culture medium was discarded, and the stage-specific cells were washed with pre-warmed PBS (137 mM NaCl, 2.7 mM KCl, 10 mM Na2HPO4 and 1.8 mM KH2PO4; pH 7.4) three times. The surface proteins of the cells were labeled by 2 mM membrane-impermeable Sulfo-NHS-SS-biotin at room temperature in PBS (at pH 8.0) for 20 minutes. The biotinylation process was stopped by Tris buffered saline (TBS: 25 mM Tris base, 150 mM NaCl, pH 7.2), the solutions were discarded and the cells were washed again three times with TBS. The cells were scraped into an ice-cold hypotonic lysis buffer (20 mM Tris-HCl, 10 mM KCl, 20 mM sucrose, 10 mM iodoacetamide (IA), pH 7.4). The cells were lysed on ice manually using a plastic micro pestle and a 1 mL syringe with 26-gauge ½ inch needle. The remained intact cells and cell debris and nuclei

were pelleted at 1700× g for 5 minutes at 4 °C, and the supernatant was transferred into a 10.4 mL polycarbonate tube and centrifuged at 40,000 rpm for 1 h at 4 °C using a 70.1 Ti fixed rotor (Beckman Coulter). Biotinylated proteins were enriched in the pellet fractions, and resuspended in the 10-times diluted lysis buffer and homogenized by 25 strokes with a Potter-Elvehjem PTFE pestle in a glass tube on ice, finally stored at -20°C. The protein concentration of the membrane preparations was measured by the Lowry method. Membrane preparations with same protein content were solubilized in the presence of 0.1% (w/v) Rapigest SF Surfactant and the solutions were supplemented with 1.25 mM iodoacetamide and 1.25 mM 2,2'-Thiodiethanol. Denatured proteins were digested overnight (~16 h) at 37 °C with proteomics grade trypsin, in a 1:50 (w/w) enzyme-to-protein ratio. Digestion was stopped by heat inactivation at 95°C for 10 minutes, thereafter the biotinylated surface peptides were pulled down neutravidin agarose resin for 1h at room temperature. Non-specific peptides were removed by several washing steps. The biotinylated peptides were eluted by 10 mM Dithiothreitol in 50 mM NH4HCO3 buffer using two consecutive incubations of 30 minutes, each at 37 °C. The fractions were combined and alkylated with 25 mM iodoacetamide in dark at 37 °C for 45 minutes. The solutions were dried in a pre-heated vacuum concentrator, then the peptides desalted with a reversed-phase C18 spin column as described in a previous work (66). The samples were dried again and stored at -20°C until the mass spectrometry analysis.

#### 3.15. Mass spectrometry

Mass spectrometry analysis was performed by Zoltán Szabó.

All measurements were carried out on a Waters ACQUITY UPLC M-Class LC system (Waters, Milford, MA, United States) coupled with an Orbitrap Exploris 240 mass spectrometer (Thermo Fisher Scientific, Waltham, MA, United States). Peptides were eluted from a C18 capillary column by an acetonitrile/water gradient in 80 minutes. Data were collected using the data-dependent acquisition (DDA) method in the 360 and 2200 Th range with a 3 s cycle time. Raw LC–MS data files were processed using Fragpipe v22.0. Uniprot Human reference proteome assuming 2 missed cleavages and Met oxidation, 3-(carbamidomethylthio)propanoyl Lys (effect of biotin labelling) and pyro Glu as variables and carbamidomethyl Cys as fixed modification. A contaminants database was created from a labeled and enriched digest of cell medium using the same

search settings and Uniprot Bovine database. Contaminant proteins and proteins with only one identified peptide were removed before statistical analysis. Statistical analysis of protein and peptide intensities was performed in Perseus 1.6.15. For differential expression analysis Student's t-test was used with a permutation-based false discovery rate (FDR<0.05) limit.

#### 4. Results

#### 4.1. Assay development for the analysis of therapy-induced senescence

To investigate the dynamics and biological relevance of therapy-induced senescence (TIS) in breast cancer, we adapted an *in vitro* assay previously established by our group (Figure 3A) (68). This model was initially designed to study drug-tolerant persister (DTP) cells following chemotherapy. By modeling essential elements of the tumor response to chemotherapy – including extensive cell death followed by the persistence of a small surviving subpopulation – it provided a robust and reproducible platform for analyzing treatment-resistant cell states. In that study, a single high-dose (IC<sub>30</sub>) treatment was applied for five days. It was observed that DTP cells remained non-proliferative for several weeks following drug removal, and that some of these dormant cells re-entered the cell cycle within 1-2 months and gave rise to new clones through clonal expansion. In the present study, we further optimized this assay to specifically enable the investigation of TIS, aiming to better understand its molecular characteristics and to

In the present study, we further optimized this assay to specifically enable the investigation of TIS, aiming to better understand its molecular characteristics and to examine its reversibility (Figure 3B). Cell line-specific concentrations were applied, with the treatment also lasting for 5 days. The concentrations applied were determined based on preliminary cytotoxicity dose-response experiments, in which 1 million cells were seeded per flask and treated with a range of drug concentrations. The selected doses induced over 90% cell death over time, while still allowing repopulation. A key difference, however, is that in this study the characterization was performed on day 12 following treatment, as by this timepoint all surviving cells had entered TIS – a conclusion that will be confirmed in the following sections of this thesis. In addition to characterizing the TIS state, we also examined repopulating (REPOP) cells, which had re-entered the cell cycle after escaping senescence. In a subset of cytotoxicity experiments, REPOP cells were subjected to a second round of treatment, allowing further analysis of a re-therapy-induced senescent (re-TIS) state.

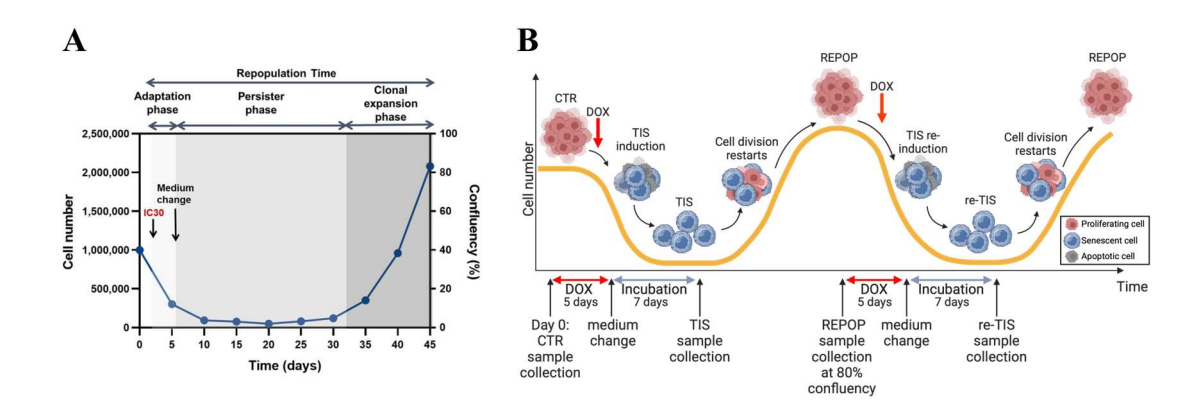


**Figure 3.** Schematic overview of the original assay developed for the study of DTP cells (A), and its extension for the analysis of TIS, including REPOP and re-TIS states (B).

#### 4.2. TIS induction and cellular characterization

To ensure molecular diversity in our experimental model, we selected four breast cancer cell lines (MCF7, T47D, MDA-MB-231, Hs578T) representing distinct subtypes. MCF7 and T47D are luminal-type epithelial lines that express estrogen (ER<sup>+</sup>) and progesterone (PR<sup>+</sup>) receptors, MCF7 also carries wild-type TP53. In contrast, MDA-MB-231 and Hs578T are triple-negative breast cancer (TNBC) cell lines – ER<sup>-</sup>, PR<sup>-</sup>, HER2<sup>-</sup> – of basal origin and exhibit mesenchymal-like characteristics (69). These four cell lines were treated with high-dose doxorubicin (DOX) at concentrations optimized for each line (120 nM for MCF7, 70 nM for T47D, 150 nM for MDA-MB-231, and 200 nM for Hs578T). These doses resulted in extensive cytotoxicity, leaving only a small fraction of cells viable after treatment. Quantitative analysis revealed the approximate survival rates of 7.25% for MCF7, 8.2% for T47D, 1.85% for MDA-MB-231, and 0.29% for Hs578T (Figure 4A). The surviving cells exhibited characteristic morphological hallmarks of senescence, including enlarged nuclei and cell bodies, a flattened morphology, increased cytoplasmic volume, and demonstrated senescence-associated β-galactosidase (SA-β-Gal) activity, as indicated by positive X-gal staining (Figure 4B). Although senescence is traditionally considered a terminal growth arrest, proliferative escape was consistently observed in each of the examined cell lines in all experiments. A small fraction of cells exited the TIS state and gave rise to REPOP populations. As these REPOP cells emerged, X-gal staining was no longer detectable in REPOP cultures and was comparable with that seen in control (CTR) populations (Figure 4B).

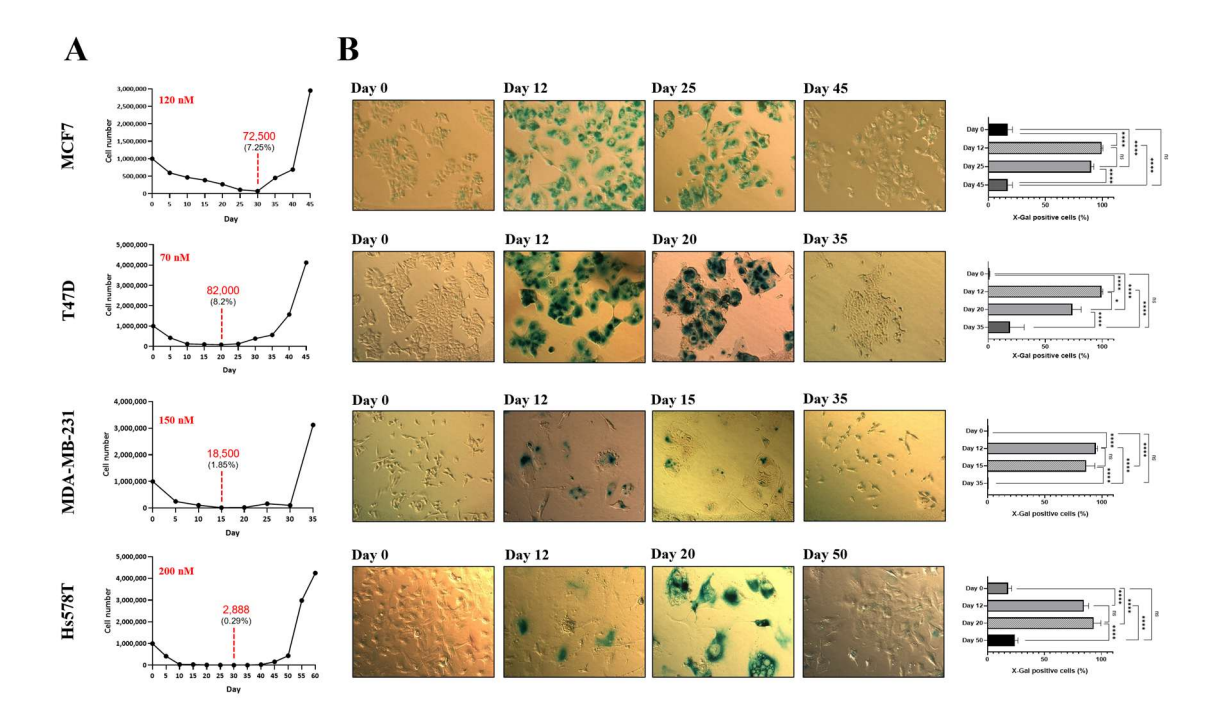


**Figure 4.** (A) Representative growth kinetics of breast cancer cell cultures following a 5-day treatment with high-dose DOX. DOX was administered on day 0, and the medium was replaced on day 5. The lowest recorded cell counts following treatment are indicated on each curve in red. (B) Detection of SA- $\beta$ -Gal activity by X-gal staining in CTR, TIS, and REPOP cells; quantification of staining intensity is also shown.

In addition to morphological and enzymatic hallmarks of senescence, we applied a multimarker approach by extending our analysis to include molecular indicators of TIS. Elevated expression of the cyclin-dependent kinase inhibitor CDKN1A (p21) was observed, along with reduced levels of LMNB1 (Lamin B1), a structural component of the nuclear lamina (Figure 5A). Furthermore, these cells displayed persistent DNA damage, as well as increased mitochondrial and lysosomal content. The formation of a single, enlarged and fused nucleolus was also noted (Figure 5B).

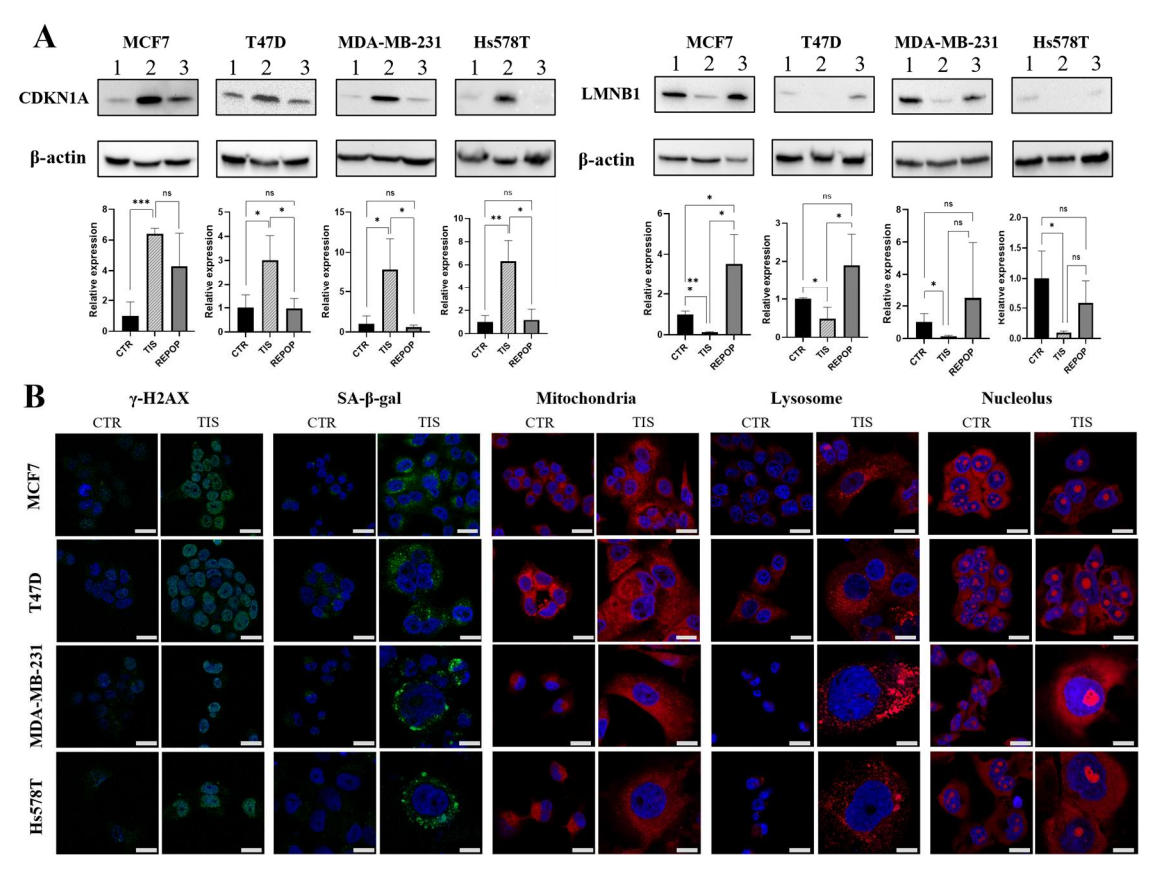
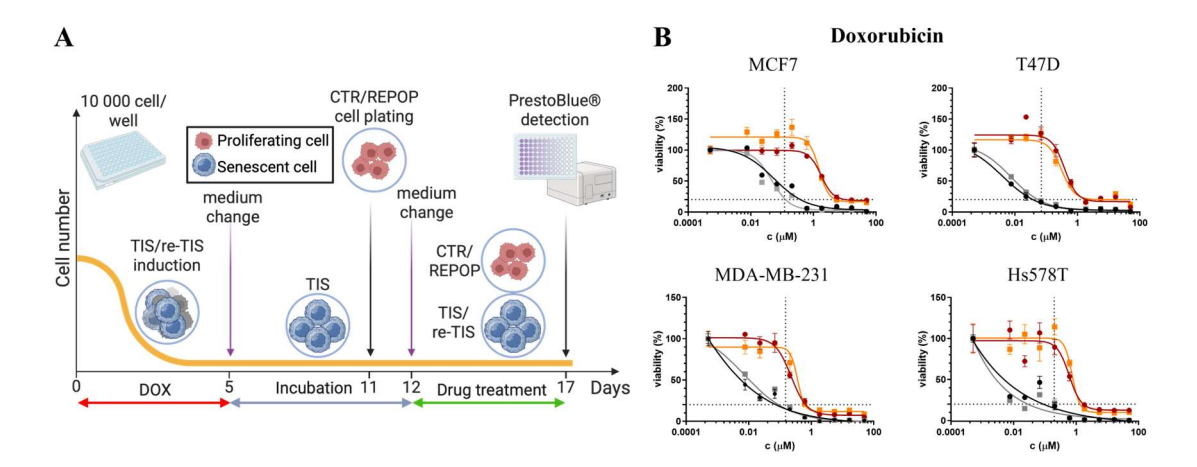


Figure 5. (A) Western blot analysis of the senescence marker CDKN1A (p21) and LMNB1 (Lamin B1) in CTR, TIS, and REPOP cells. Quantification of relative protein expression levels is presented alongside the blots. (B) Fluorescence microscopy-based detection of key cellular senescence features in CTR and TIS cells. Scale bar: 20 µm.

#### 4.3. Drug resistance and sensitivity profile of TIS breast cancer cells

Since chemotherapy is typically administered in multiple cycles in clinical settings, we aimed to assess how TIS cells respond to repeated drug exposure. For this, we developed a protocol that enabled us to monitor the drug sensitivity not only on CTR and TIS, but REPOP and re-TIS states as well using cytotoxicity assays (Figure 6A). Notably, TIS cells exhibited marked resistance to a second round of DOX (Figure 6B). However, this resistance was not sustained once the cells exited the TIS state. Following repopulation, sensitivity to DOX was restored, indicating that drug resistance was closely linked to the TIS phenotype. To further test this, REPOP cells were re-exposed to DOX. As a result, re-TIS state successfully reinstated drug resistance, demonstrating that the TIS program itself is capable of transiently protecting breast cancer cells against repeated chemotherapy.



**Figure 6. (A)** Schematic illustration of the experimental design, highlighting the timeline of senescence induction, recovery phases, and subsequent drug screening steps. **(B)** DOX response curves for CTR (black), TIS (red), REPOP (gray), and re-TIS (orange) cell populations.

To better understand the clinical relevance of the drug-resistant phenotype seen in TIS cells, we tested several chemotherapeutic agents that are widely used in breast cancer treatment (Figure 7). This included gemcitabine, an antimetabolite, as well as paclitaxel and docetaxel, two commonly used taxanes. These drugs were able to eliminate both CTR and REPOP cells effectively, but were ineffective against TIS and re-TIS cells.

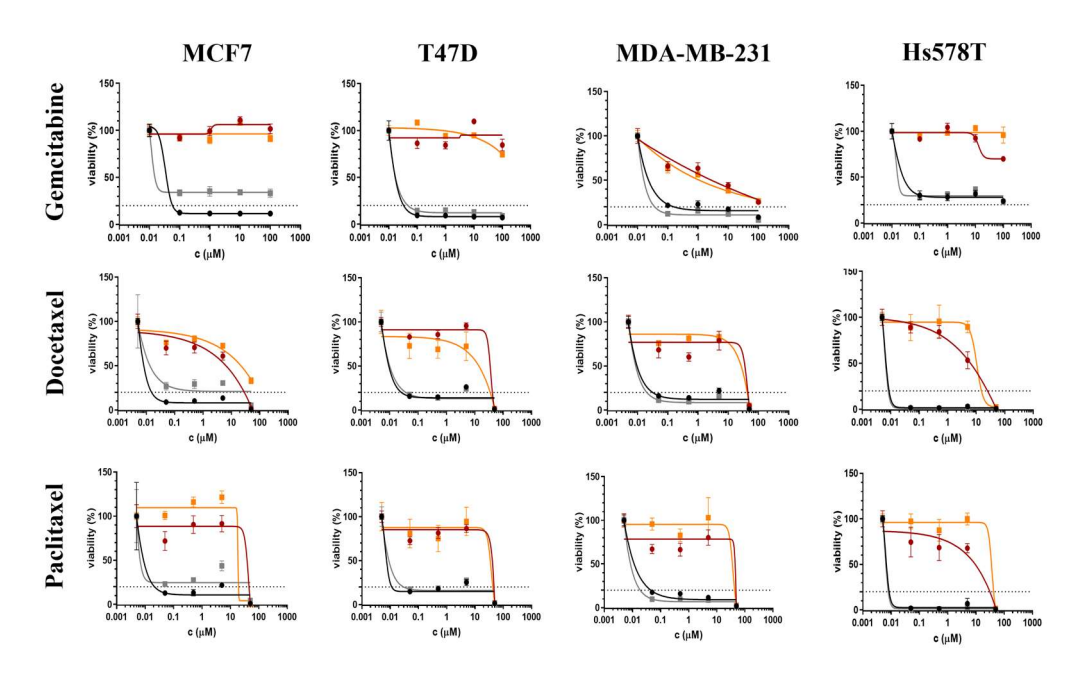


Figure 7. Comparison of drug responses across CTR (black), TIS (red), REPOP (gray), and re-TIS (orange) cells treated with commonly used breast cancer therapies.

To explore whether TIS cells exhibit resistance to a broader range of drugs, we conducted a drug screen using 63 FDA-approved agents. TIS cells exhibited resistance to several drug classes, including antimetabolites (5-azacytidine, 5-fluoro-2'-deoxycytidine, cladribine, cytarabine, clofarabine and troxacitabine), topoisomerase II inhibitors (mitoxantrone, pixantrone, voreloxin), polo-like kinase 1 inhibitors (volasertib), alkylating agents (chlormethine, chlorambucil, and melphalan), a neddylation inhibitor (pevonedistat), a farnesyltransferase inhibitor (tipifarnib) and an FLT3 inhibitor (gilteritinib). (Figure 8A). Notably, the FLT3 inhibitor quizartinib remained effective despite TIS resistance to gilteritinib. In contrast, some compounds, such as HDAC inhibitors (belinostat, HDAC-42, panobinostat, pracinostat, ricolinostat, romidepsin, vorinostat), PI3K inhibitors (duvelisib), and proteasome inhibitors (bortezomib, ixazomib), showed similar response across CTR and TIS cells. Importantly, the observed resistance in TIS cells does not appear to result solely from their non-proliferative state, as certain drugs that require active cell division still remain effective. For instance, although dinaciclib was ineffective, other multi-CDK inhibitors such as AT7519 and SB-1317 induced cell death in both proliferating and senescent cells. Similarly, the BTK inhibitor ibrutinib, as well as several multi-tyrosine kinase inhibitors (masitinib, nintedanib, sorafenib, sunitinib) were active in the majority of cell lines. In contrast, crenolanib showed no efficacy against TIS cells.

Altogether, TIS cells exhibited resistance to 23 of the 46 active agents in at least three out of four breast cancer cell lines, while 17 out of the 63 tested compounds showed no cytotoxic activity at the applied concentrations in either TIS or CTR cells. These results indicate that TIS is associated with a distinct and potentially clinically relevant drug resistance phenotype.

Hierarchical clustering was performed using the IC<sub>50</sub> values of 46 compounds (Figure 8B). The analysis revealed a clear separation between CTR and TIS samples across all breast cancer cell lines, supporting the presence of a distinct drug response profile in TIS. Mechanistically related compounds tended to cluster together, reflecting consistent activity patterns. For example, topoisomerase II inhibitors (voreloxin, pixantrone, mitoxantrone), antimetabolites (cytarabine, troxacitabine, clofarabine, 5-azacytidine, cladribine; excluding 5-fluoro-2'-deoxycytidine), HDAC inhibitors (romidepsin, HDAC-42, belinostat, panobinostat, pracinostat, ricolinostat; excluding vorinostat), proteasome

inhibitors (bortezomib, carfilzomib; excluding ixazomib), and multi-CDK inhibitors (SB-1317, dinaciclib; excluding AT-7519) displayed coherent clustering across conditions. In contrast, multi-tyrosine kinase inhibitors (sunitinib, masitinib, nintedanib, crenolanib, and sorafenib) exhibited heterogeneous clustering patterns, suggesting divergent cellular responses despite overlapping molecular targets.

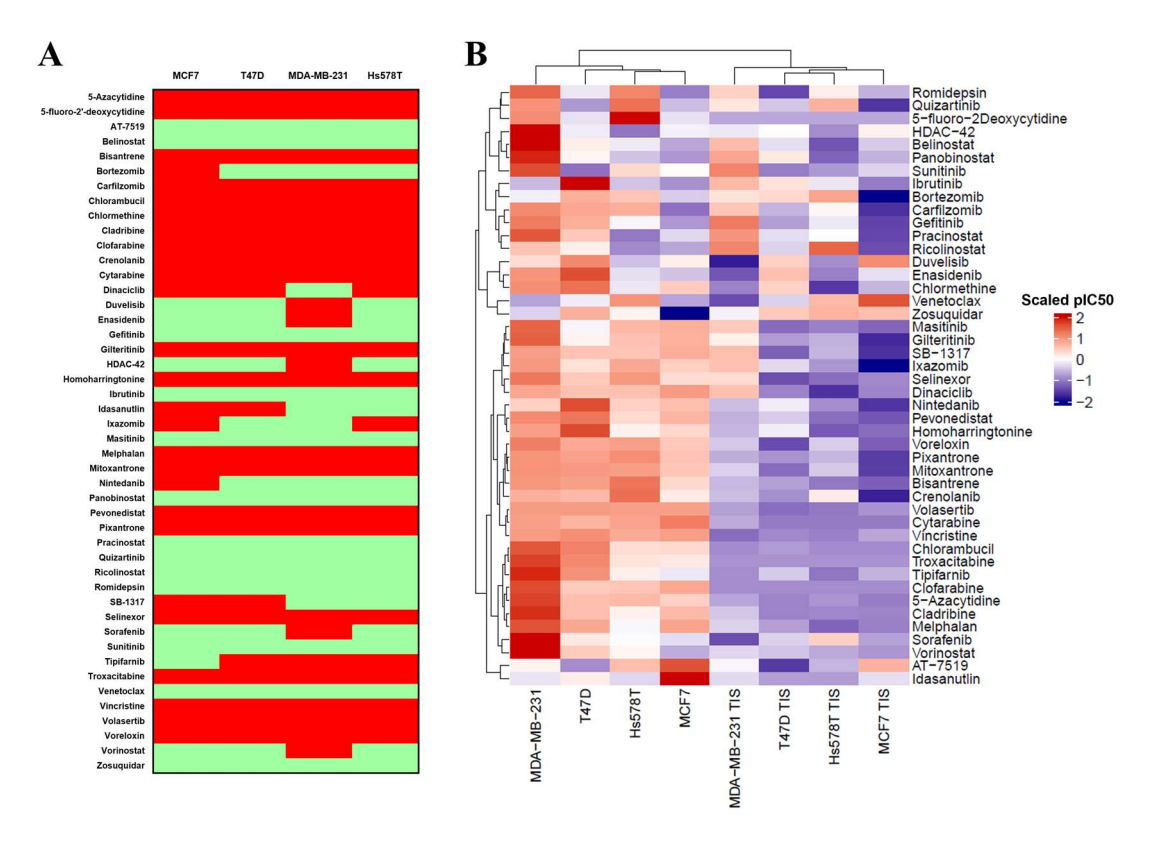


**Figure 8.** (A) Heatmap representing the drug response profile of TIS cells relative to CTR cells across a panel of 46 FDA-approved anticancer drugs. Increased resistance ( $\geq$ 3-fold) in TIS is highlighted in red; drugs with similar effects in both cell states are shown in green. (B) Heatmap of IC50 values, centered and scaled for each drug individually. Hierarchical clustering was performed using Euclidean distance and Ward's method.

To confirm that the TIS state alone is sufficient to confer protection against repeated chemotherapy exposure, we compared the drug sensitivity profiles of TIS and re-TIS cells. For this, cells were treated with a panel of 15 compounds previously found to be ineffective in all four cell lines during the TIS state (Figure 9). The drug response pattern observed in re-TIS cells closely resembled that of the original TIS populations, supporting the notion that TIS itself is capable of transiently maintaining drug resistance.

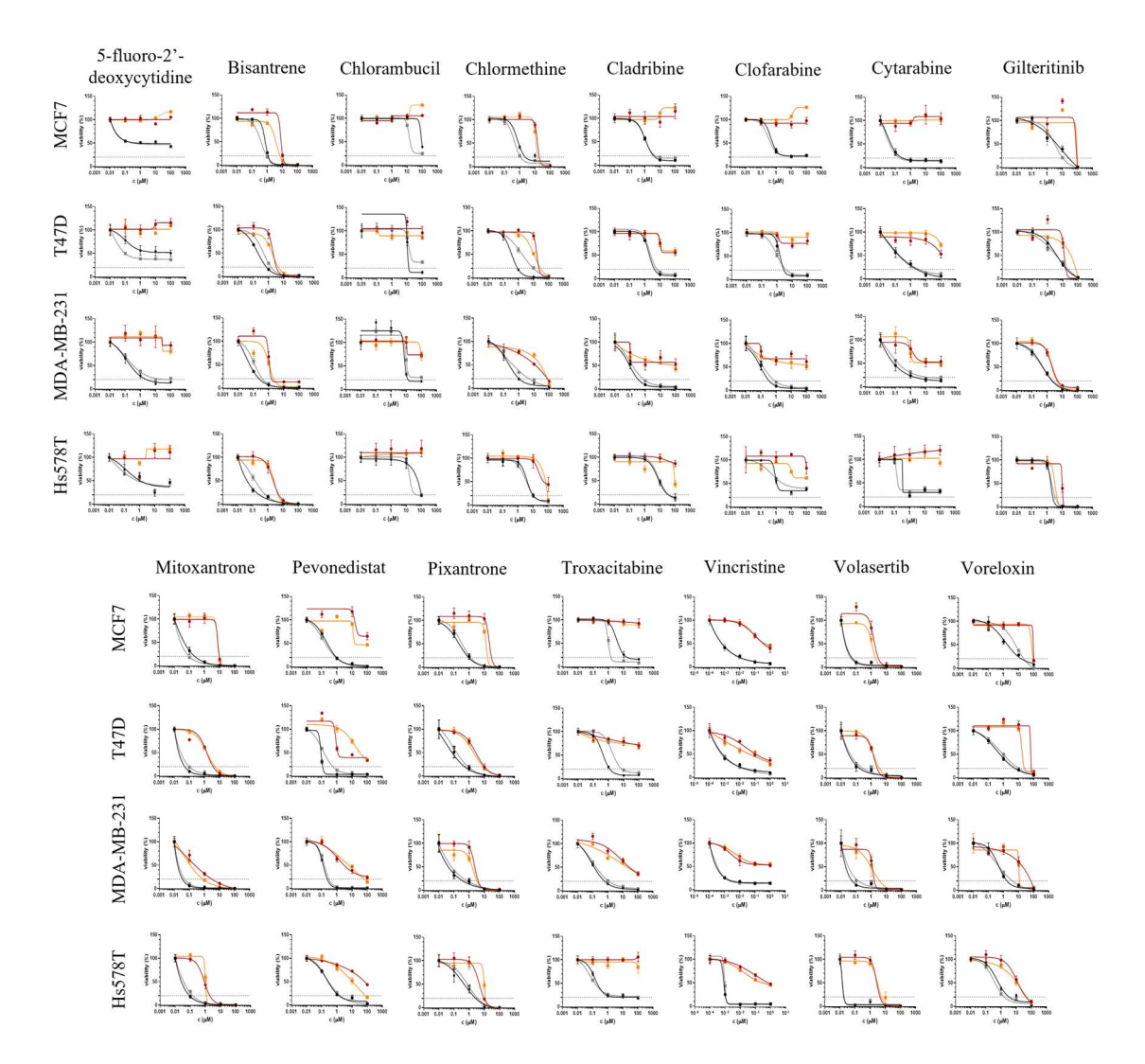


**Figure 9.** Sensitivity analysis of CTR (black), TIS (red), REPOP (gray), and re-TIS (orange) cells treated with 15 compounds selected from those that had previously induced resistance in all four cell lines. Concentration range:  $100\mu M/10$  (except Vincristine:  $1\mu M/10$ ).

Based on our findings, TIS cells exhibited broad and reproducible resistance to multiple classes of chemotherapeutic agents, including standard drugs used in breast cancer treatment. This resistance was shown to be reversible, as drug sensitivity was restored upon exit from TIS and re-established after re-induction. The consistency of these patterns across cell lines and treatment conditions suggests that the TIS state alone is sufficient to confer a distinct and clinically relevant drug-resistant phenotype.

#### 4.4. Investigation of the response of TIS cells to senolytic treatments

#### 4.4.1. Response to the senolytic agent Navitoclax

To explore whether senescent cells could be selectively targeted and eliminated during chemotherapy, we focused on navitoclax, a well-characterized Bcl-2 family inhibitor that has been widely studied for its senolytic potential. Given the continued uncertainty regarding how specifically Bcl-2 inhibitors act on senescent cells, we designed a combinatorial treatment approach in which navitoclax was administered alongside DOX during the induction of TIS. The aim was to determine whether depleting TIS cells during this phase could prevent subsequent repopulation. In short-term cytotoxicity assays, navitoclax showed clear senolytic activity (Figure 10).

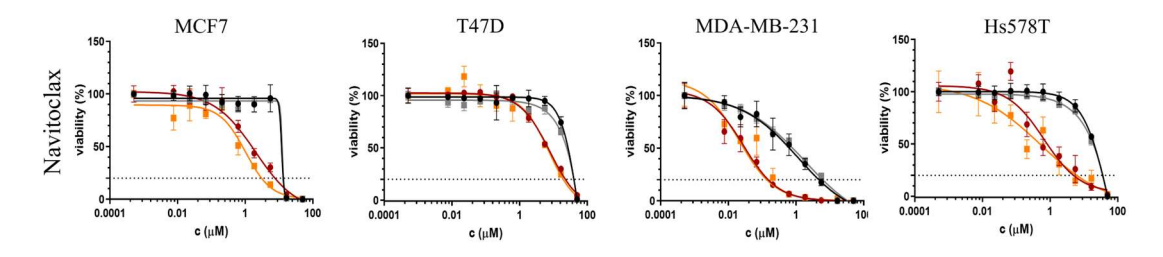


**Figure 10.** Dose-response curves showing the sensitivity of CTR (black), TIS (red), REPOP (gray), and re-TIS (orange) cells to navitoclax treatment.

The aim was to determine whether depleting TIS cells during this phase could prevent subsequent repopulation. However, the results of longer treatments were inconsistent, ranging from complete elimination of cells to no noticeable effect. (Figure 11). Our results indicate that navitoclax must be present from the start of DOX treatment to effectively reduce relapse, implying that Bcl-2 upregulation may occur as an early response to chemotherapy rather than as a senescence-specific adaptation.

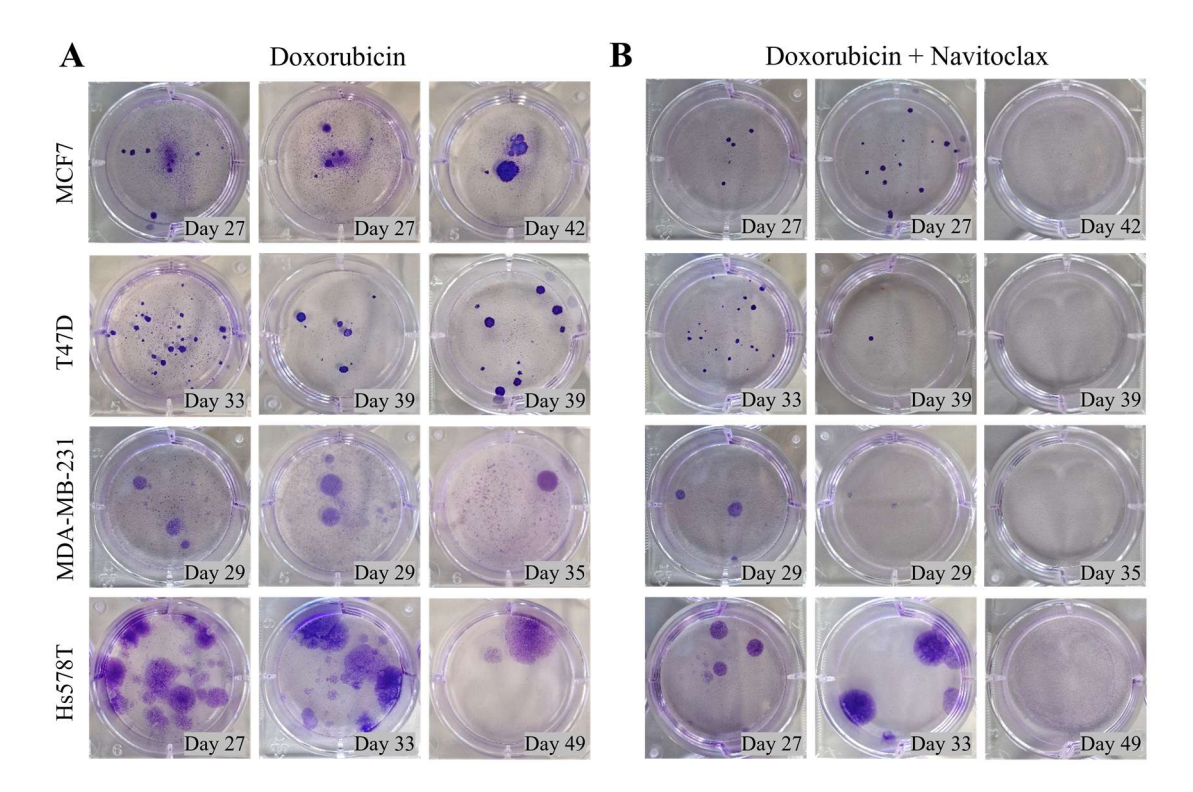


**Figure 11.** Representative crystal violet staining of breast cancer cell cultures treated with DOX alone **(A)** or in combination with navitoclax (DOX + navitoclax) **(B)**, illustrating long-term treatment outcomes.

To validate our *in vitro* findings in an *in vivo* context, we selected a clinically relevant mouse model of triple-negative breast cancer (TNBC), in which a single dose of pegylated liposomal doxorubicin (DOXIL) resulted in complete tumor regression (Figure 12A). In this model, the absence of detectable or palpable tumors was maintained for a period of 40 to 60 days following treatment (Figure 12B), which was consistent with the response observed *in vitro*. Subsequent treatment with navitoclax, however, did not improve therapeutic outcomes. No significant difference in tumor relapse time was observed between the DOXIL and the DOXIL-navitoclax groups (Figure 12C), and overall survival remained unchanged (Figure 12D). These results highlight the limited therapeutic potential of navitoclax in this setting, despite its previously reported senolytic activity.

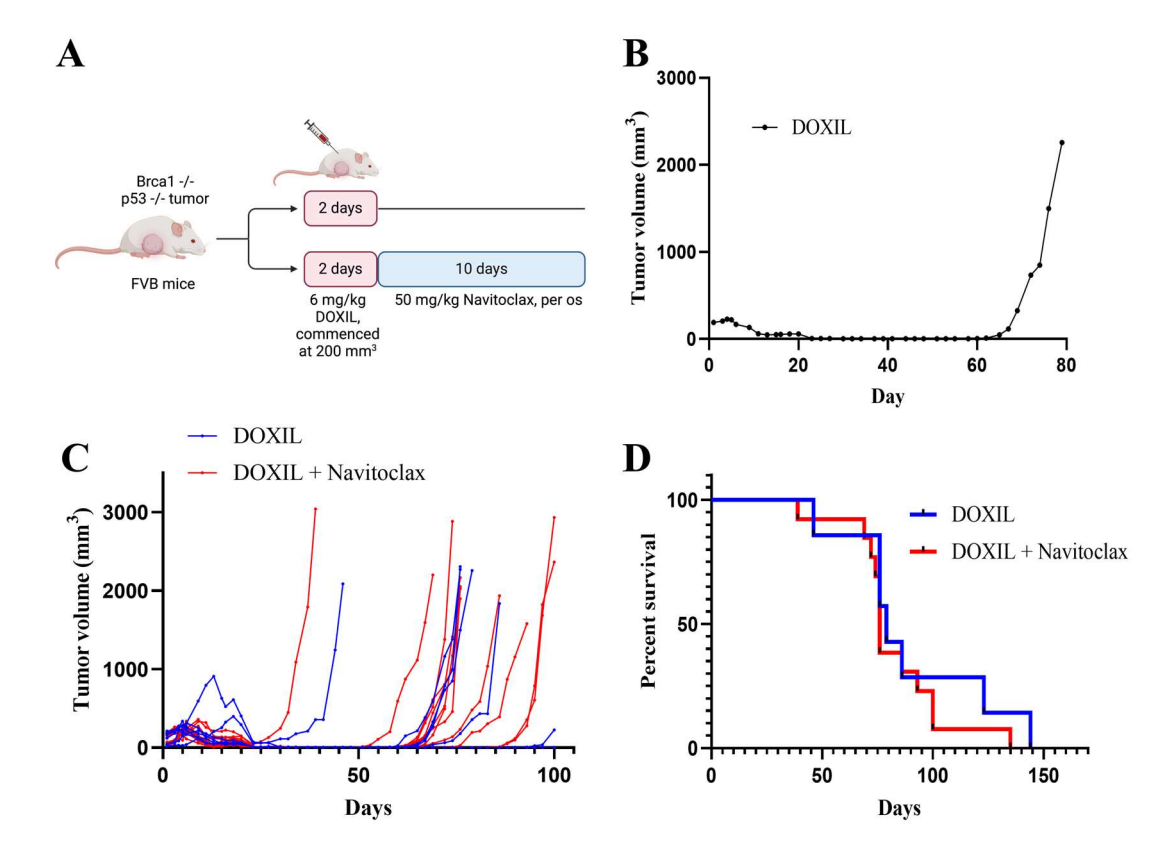
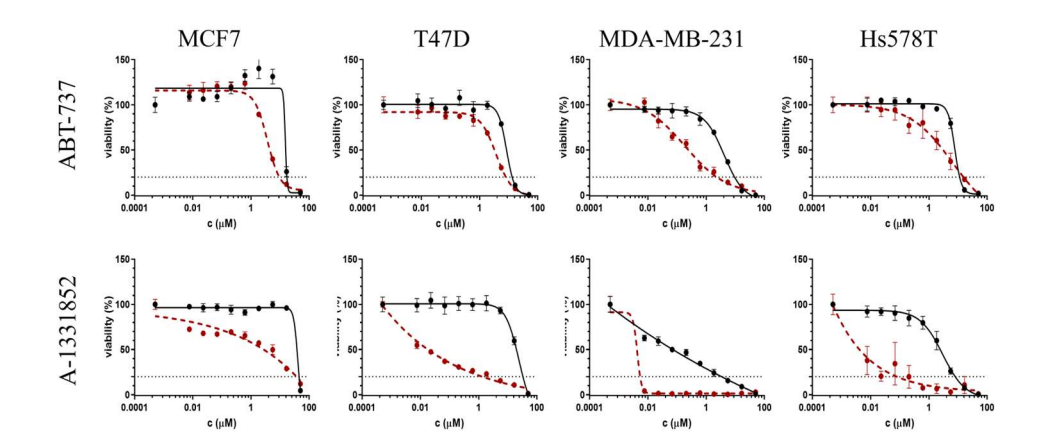


Figure 12. (A) Schematic representation of the experimental design used to compare DOXIL monotherapy with the combination of DOXIL and navitoclax in an in vivo TNBC model. (B) Representative tumor growth curve of  $Brca1^{-/-};p53^{-/-}$  tumors following treatment with the maximum tolerated dose of DOXIL. (C) Tumor growth curves of individual  $Brca1^{-/-};p53^{-/-}$  mice treated with DOXIL (n = 7) or DOXIL + navitoclax (n = 13). (D) Kaplan—Meier survival analysis of  $Brca1^{-/-};p53^{-/-}$  tumor-bearing mice treated with DOXIL (n = 7) or DOXIL + navitoclax (n = 13). Statistical comparison revealed no significant difference between groups (p = 0.3888).

### 4.4.2. Response to additional senolytic compounds

To further investigate the sensitivity of TIS cells to additional senolytic compounds, we tested a panel targeting diverse molecular pathways, including several Bcl-family inhibitors. ABT-737 (Bcl-2/Bcl-XL) and A-1331852 (Bcl-XL) selectively reduced the viability of TIS cells, suggesting a key role for Bcl-XL in apoptosis resistance (Figure 13). In contrast, venetoclax (Figure 8A), a selective Bcl-2 inhibitor, showed similar toxicity in CTR and TIS cells, indicating no selective senolytic effect.



**Figure 13.** Cytotoxicity assay of CTR (black) and TIS (red) cells to the senolytic agents ABT-737 and A-1331852.

To determine whether differential expression of Bcl family proteins could explain these observations, we analyzed their expression and localization during and after doxorubicin treatment. However, neither protein expression level nor subcellular distribution correlated with drug sensitivity (Figure 14A, B).

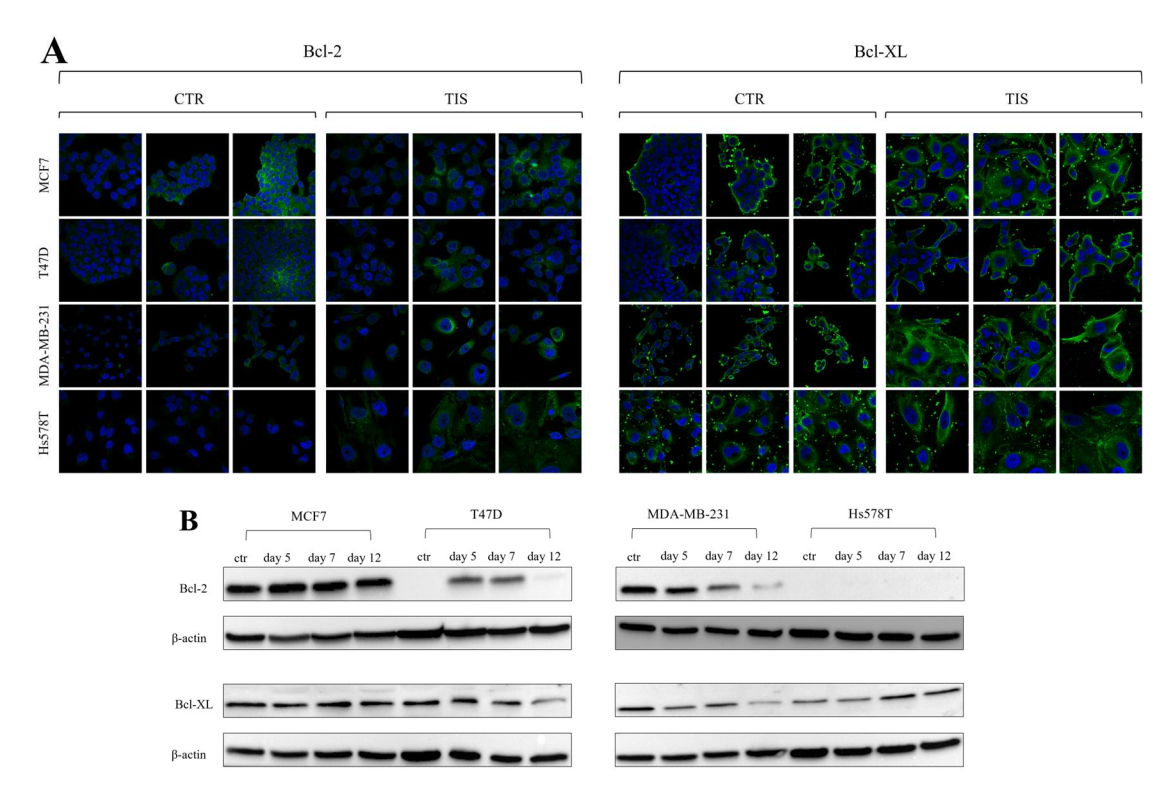


**Figure 14.** (A) Comparative evaluation of Bcl-2 and Bcl-XL expression intensity, localization, and cellular heterogeneity in CTR and TIS cells on day 12 of senescence induction. (B) Western blot analysis of Bcl-2 and Bcl-XL expression during a 12-day TIS induction protocol, showing temporal changes associated with senescence progression.

We also tested additional senolytic agents, including dasatinib, fisetin, quercetin, and piperlongumine, which were previously reported to selectively eliminate senescent cells. However, TIS cells in our system did not exhibit increased sensitivity to these agents; in fact, in most cases, they showed resistance (Figure 15).

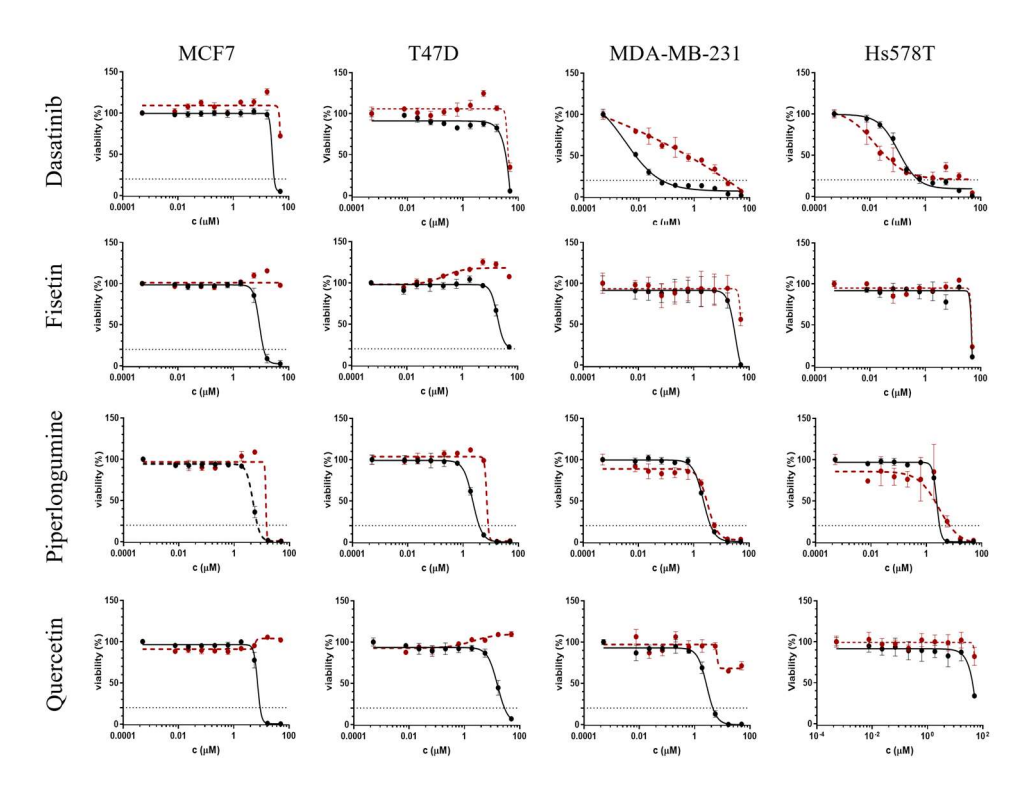


*Figure 15.* Cytotoxicity assay of CTR (black) and TIS (red) cells to the senolytic agents dasatinib, fisetin, piperlongumine and quercetin.

### 4.5. Bulk RNA sequencing analysis of TIS

To characterize the transcriptional features of the TIS state across four breast cancer cell lines, we performed bulk RNA sequencing (bulk RNA-seq) and analyzed differentially expressed genes (DEGs). The bioinformatic processing and analysis of the bulk RNA-seq data were performed by Anna Lovrics. For each cell line, we included samples representing all three cellular states (CTR, TIS, and REPOP).

Although gene expression patterns varied between cell lines, 929 genes were found to be commonly differentially expressed in TIS compared to CTR cells (Figure 16A, B). Of these, 896 (96.5%) were upregulated, while only 33 genes (3.5%) were downregulated. In contrast, the transition from TIS to REPOP involved 722 differentially expressed genes, with 706 (97.8%) downregulated and only 16 (2.2%) upregulated (Figure 16C, D).

When CTR and REPOP cells were compared, only one gene (IFIT1) remained upregulated in all cell lines, and no genes were consistently downregulated (Figure 16E, F). These findings indicate that TIS is associated with strong transcriptional activation, which is reversed upon exit from senescence and restoration of proliferative capacity. This bidirectional regulation underscores the dynamic and reversible nature of the TIS-associated transcriptome.

To identify TIS-specific genes, we selected transcripts upregulated during senescence and downregulated upon re-entry into the cell cycle. This analysis identified 316 mRNAs transiently elevated during TIS. Although REPOP and CTR cells showed similar transcriptomes – only IFIT1 was consistently upregulated across all four cell lines – 22 additional genes showed persistent overexpression in at least three cell lines.

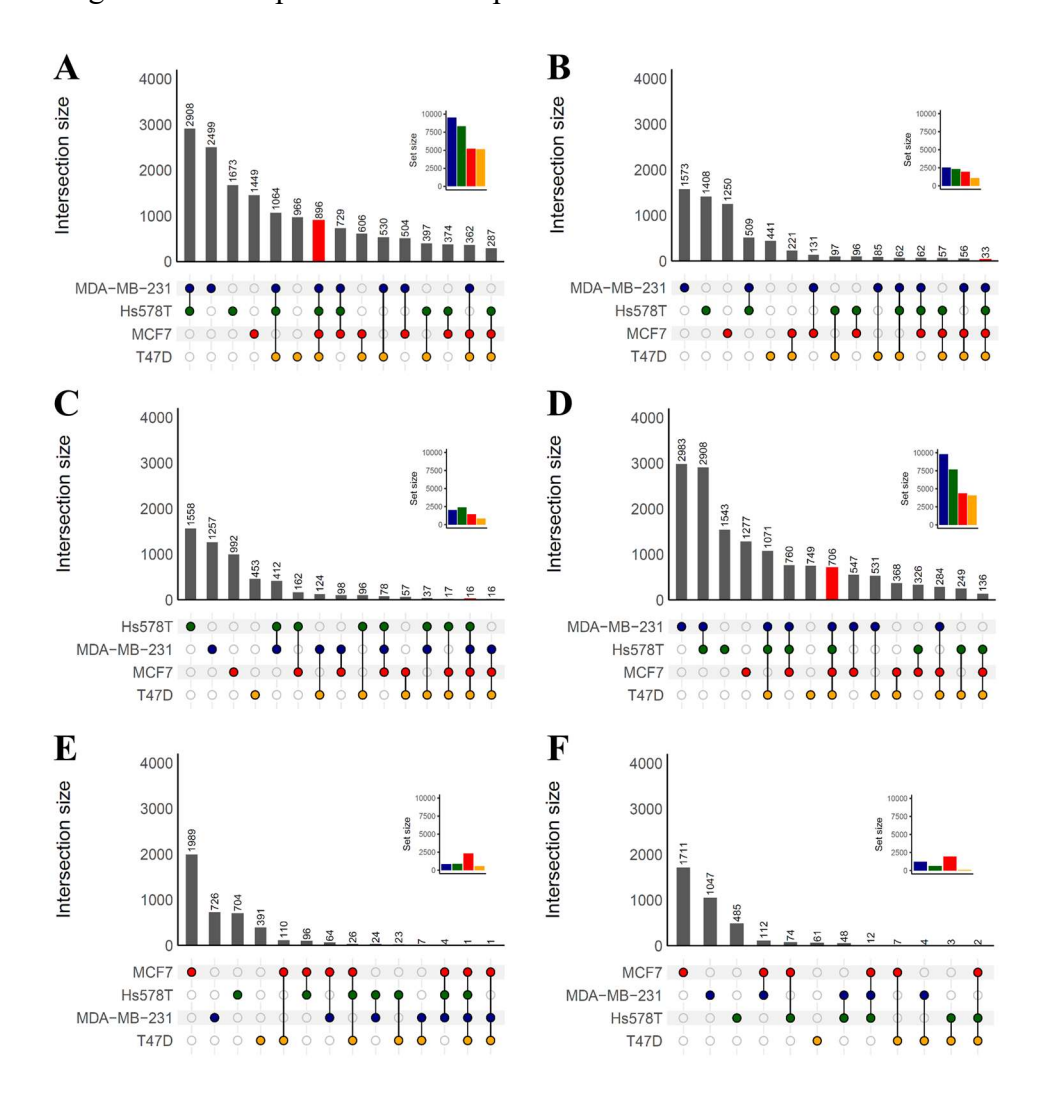


Figure 16. (A, B) UpSet plots showing the overlap of DEGs identified in CTR vs. TIS comparisons. Panel (A) displays upregulated genes, while panel (B) shows downregulated genes. Red bars indicate genes commonly altered across all four cell lines. (C, D) UpSet plots of DEGs from TIS vs. REPOP comparisons, highlighting upregulated (C) and downregulated (D) genes. Shared DEGs detected in all cell lines are marked in red. (E, F) UpSet plots of DEGs from CTR vs. REPOP comparisons, illustrating upregulated (E) and downregulated (F) genes.

# 4.5.1. Pathway analysis

To identify shared molecular features of the TIS phenotype, gene set enrichment analysis (GSEA) was performed on the mRNA expression data (Figure 17A). The analysis identified several characteristic pathways associated with the TIS state. TIS cells exhibited markedly reduced proliferative activity, as five out of six proliferation-related gene sets from the Molecular Signatures Database (MSigDB) "hallmark" collection – including G2M Checkpoint, E2F Targets, MYC Targets V1 and V2, and Mitotic Spindle – were significantly downregulated. The only exception was the p53 pathway, which remained unchanged. The DNA Repair gene set was also suppressed, indicating a reduced capacity for maintaining genomic integrity during senescence. Furthermore, all seven immune-related hallmark gene sets – including Allograft Rejection, Coagulation, Complement, Interferon alpha and gamma responses, IL6-JAK-STAT3 signaling, and Inflammatory Response – showed differential regulation, indicating that the TIS state may be associated with substantial alterations in immune-related signaling pathways. Importantly, all of these transcriptional changes were reversed in REPOP cells following escape from senescence (Figure 17B).

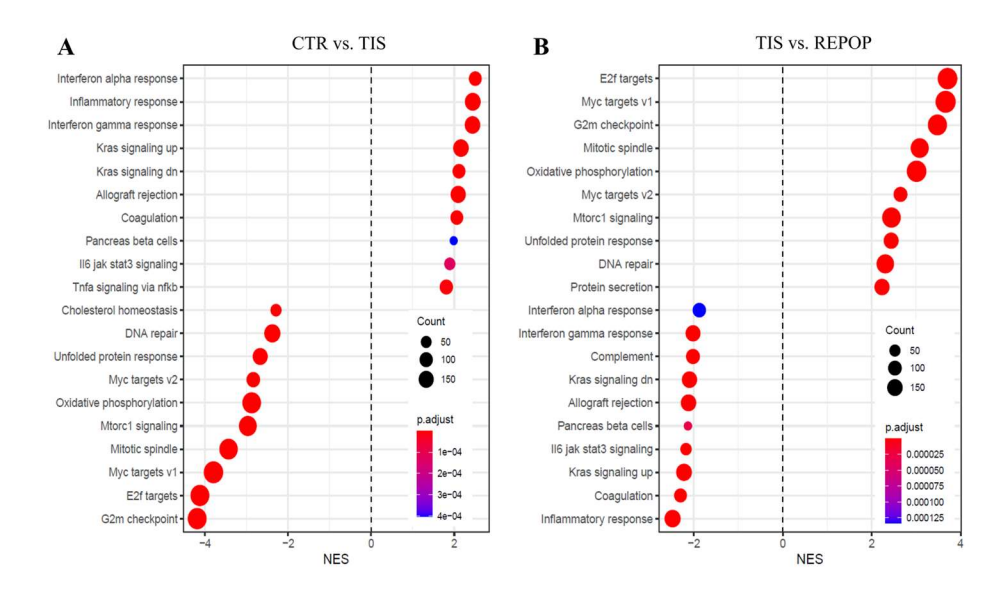


Figure 17. Gene set enrichment analysis (GSEA) of RNA-seq data from MCF7, T47D, MDA-MB-231, and Hs578T cells, displaying the top 10 positively and negatively enriched pathways based on normalized enrichment scores (NES). Panel (A) shows pathway alterations in CTR vs. TIS comparisons, while panel (B) represents changes observed between TIS and REPOP states.

# 4.5.2. Drug resistance analysis

To explore potential mechanisms underlying the drug resistance observed in TIS cells, we examined the expression of known drug resistance genes, including efflux transporters, DNA repair factors, and targets of the tested compounds (Figure 18A). In most cases, gene expression patterns did not correlate with drug sensitivity or resistance. For example, although CDK1,2,4,5,7, and 9 are targets of multi-CDK inhibitors (AT7519, SB-1317, dinaciclib), no consistent link was observed between their expression and CDK inhibitor response. Similarly, the loss of FDPS or the overexpression of BCL2, which are associated with sensitivity to tipifarnib or venetoclax, respectively, did not explain resistance patterns in TIS cells (70, 71).

While increased expression of RRM1/2/2B is commonly linked to resistance against agents like DOX (72), gemcitabine, and docetaxel, these genes were found to be downregulated in TIS cells. Similarly, although SAMHD1 and DCK are known mediators of antimetabolite resistance (73-75), only SAMHD1 showed moderate upregulation, and only in two cell lines. Additionally, the expression of genes targeted by several biologic therapies – such as FLT3 (crenolanib, gilteritinib, quizartinib), EGFR (gefitinib), BTK

(ibrutinib), MDM2 (idasanutlin), FGFR1 (nintedanib), and PSMB5 (bortezomib, ixazomib) – was not upregulated in TIS cells. In some cases, even when targets like NEDD8 (targeted by pevonedistat (76)) were upregulated, this did not result in increased drug sensitivity. Conversely, downregulation of genes such as IDH2 (targeted by enasidenib) did not lead to resistance.

A few notable exceptions were identified. Downregulation of XPO1 and PLK1 may explain resistance to selinexor and volasertib, respectively (77, 78). Reduced expression of DNMT1, DNMT3A/3B was detected in TIS cells, potentially limiting the efficacy of DNMT inhibitors (5-azacytidine, 5-fluoro-2'-deoxycytidine) (79, 80). Similarly, TOP2A downregulation may contribute to resistance against DOX, mitoxantrone, pixantrone and voreloxin. Among drug efflux transporters, ABCB1 and ABCG2 were consistently upregulated in all TIS models, while ABCC1 and ABCC3 were cell line-specific. Despite the high expression of ABCB1 in TIS cells, resistance to several known substrates of this transporter (81) – including belinostat, bortezomib, gefitinib, sorafenib, and sunitinib – was not observed. To test whether ABCB1 plays a functional role, we inhibited it with tariquidar and assessed doxorubicin sensitivity (Figure 18B). The treatment had no detectable effect, indicating that ABCB1 overexpression alone is insufficient to protect TIS cells from chemotherapy.

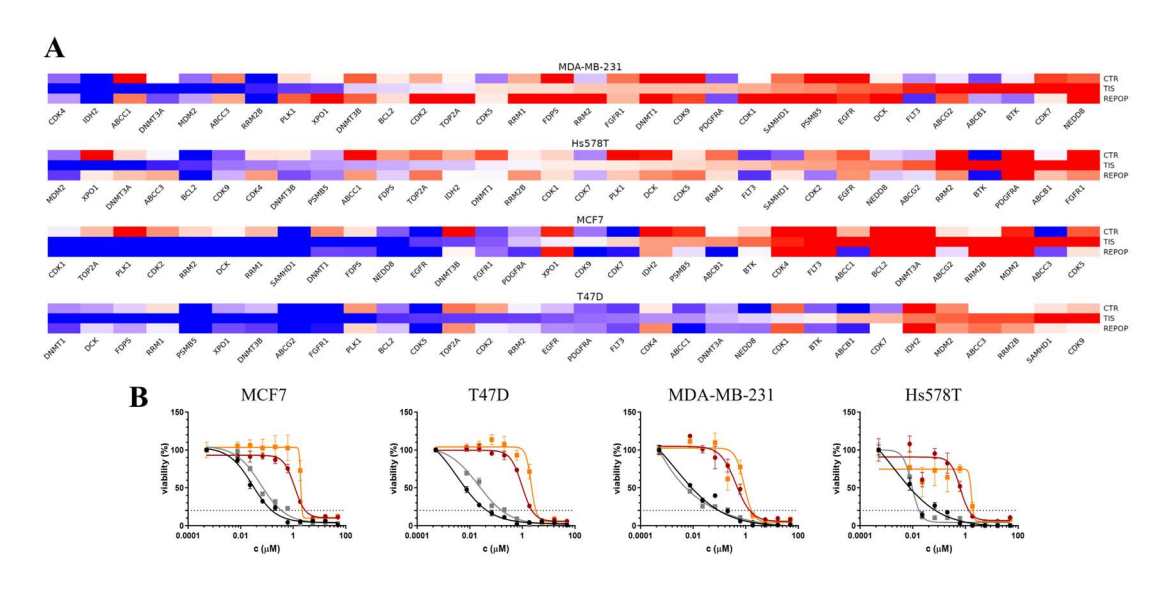


Figure 18. (A) Heatmap showing scaled expression patterns of genes linked to resistance mechanisms for the tested compounds. For each gene, expression values were centered and normalized across all samples to highlight relative changes. (B) Effect of ABCB1 inhibition on DOX sensitivity in CTR and TIS cells. DOX response was measured in the

absence or presence of 1  $\mu$ M tariquidar, a third-generation ABCB1 inhibitor. CTR cells are shown in black (without inhibitor) and gray (with tariquidar); TIS cells in red (without inhibitor) and orange (with tariquidar).

### 4.6. Single-cell RNA sequencing analysis of TIS

To gain a deeper understanding of TIS, we performed single-cell RNA sequencing (scRNA-seq) on MCF7 and T47D breast cancer cell lines. This allowed detailed examination of cell state transitions in response to therapy at the single-cell level, capturing molecular changes associated with entry into and escape from TIS. The bioinformatic processing and analysis of the scRNA-seq data were performed by Csaba Kiss and Sándor Spisák. To validate the quality of the scRNA-seq datasets, the consistency between biological replicates was assessed, and pseudo-bulk expression patterns were compared to those from bulk RNA-seq (Figure 19A,B). Gene expression profiles were consistent across replicates, and the similarity between pseudo-bulk and bulk data confirmed the reliability of the scRNA-seq results.

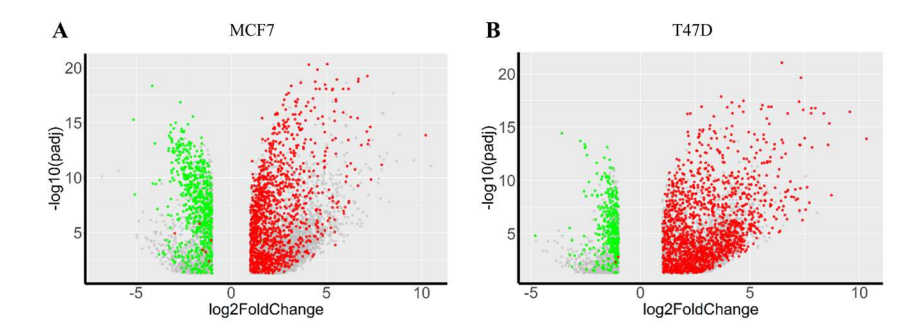


Figure 19. (A,B) Comparison of pseudo-bulk RNA-seq data generated from scRNA-seq with bulk RNA-seq results for MCF7 (A) and T47D (B) cell lines. The analysis demonstrates consistency between single-cell and bulk transcriptomic profiles, with red indicating upregulated and green indicating downregulated genes.

# 4.6.1. Clustering analysis of cell states

In this study, scRNA-seq data from MCF7 and T47D cell lines were analyzed using unsupervised clustering and uniform manifold approximation and projection (UMAP) (Figure 20A, B). In both models, TIS cells were found to form distinct clusters, clearly separated from CTR populations. In contrast, REPOP cells were positioned closer to CTR cells, particularly in the T47D dataset, where the two populations almost completely overlapped. These findings support the interpretation that the TIS state represents a

transient and reversible transcriptional program. In MCF7, greater heterogeneity was observed among REPOP samples. Despite being collected at the same time point, replicate datasets displayed variable clustering patterns, suggesting that the process of exiting TIS may vary between cells in terms of both timing and molecular mechanisms.

To compare the two models in a unified framework, datasets from MCF7 and T47D were integrated and jointly normalized (Figure 20C). This analysis revealed clear separation between cell lines and between cellular states. The results suggest that cell line-specific transcriptional programs play a major role in defining global gene expression patterns. At the same time, the TIS state also emerges as a strong and consistent factor, introducing a distinct signature that is clearly detectable across models. These findings indicate that both cell type and the TIS state contribute significantly to the observed transcriptomic profiles.

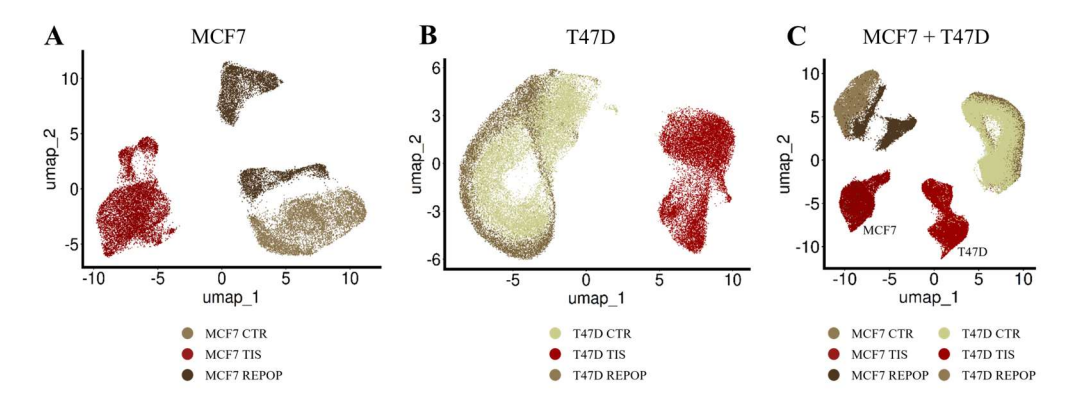
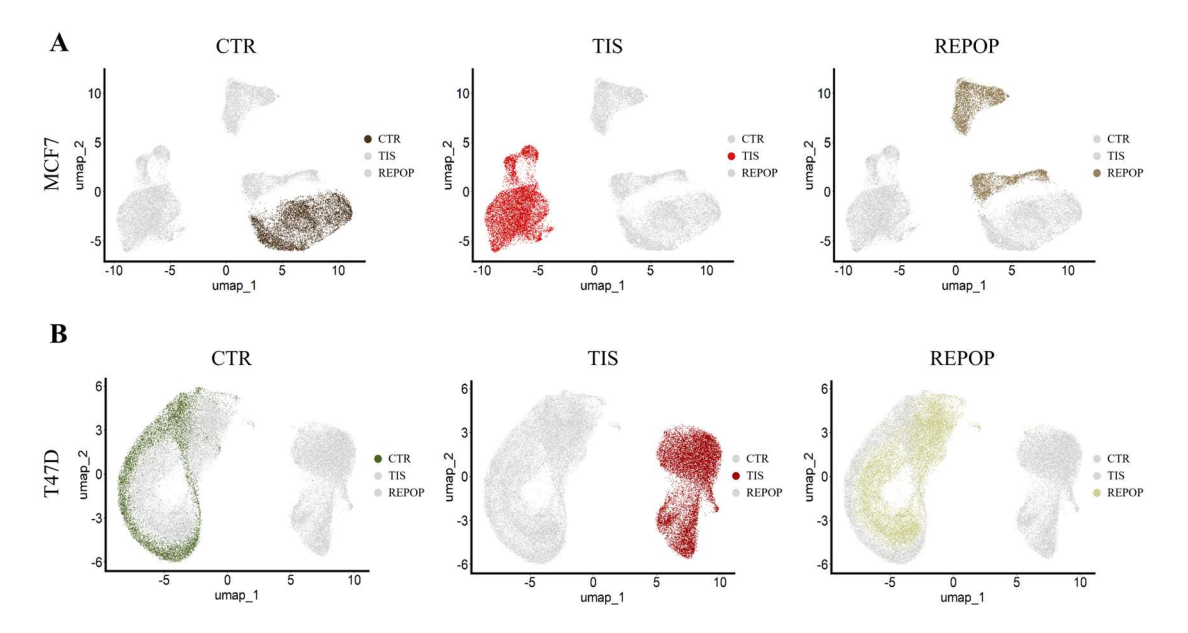


Figure 20. (A) UMAP plot of MCF7 single-cell transcriptomes showing clear separation of CTR (light brown), TIS (scarlet), and REPOP (dark brown) clusters. The REPOP population displays a partial shift toward CTR, indicating progressive reversal of the TIS-associated transcriptional program. (B) UMAP plot of T47D cells revealing clear separation between CTR (light green), TIS (crimson), and REPOP (light brown) clusters. (C) UMAP-based integration of single-cell transcriptomes from MCF7 and T47D models revealed clear differences driven by both cell identity and senescence status. CTR cells (MCF7 in light brown; T47D in light green) from each line formed separate clusters, and TIS populations (MCF7 in scarlet; T47D in crimson) also showed distinct positions relative to their corresponding controls.

The biological replicates from both MCF7 and T47D cell lines were analyzed to assess the separation of CTR, TIS, and REPOP populations (Figure 21A,B). In both models, the

three cell states formed distinct clusters, indicating consistent transcriptional differences. These findings support that REPOP cells originate from TIS cells that have regained proliferative capacity, and further indicate that their emergence is not due to the expansion of a minor subpopulation of surviving CTR cells.



**Figure 21.** UMAP projections of combined biological replicates for MCF7 (A) and T47D (B) cells, showing the distribution of CTR (dark brown for MCF7, dark green for T47D), TIS (scarlet for MCF7, crimson for T47D), and REPOP (light brown for MCF7, light green for T47D) populations.

# 4.6.2. Investigation of senescence-associated transcriptional changes

To investigate senescence-associated transcriptional changes at the single-cell level, we analyzed the expression of key regulatory genes involved in cell cycle control. The two previously examined senescence markers - upregulation of CDKN1A (Figure 22A and B, top left panels) and downregulation of LMNB1 (Figure 22A and B, bottom right panels) - showed transcript-level changes consistent with earlier protein data (Figure 5A), confirming the TIS phenotype and point to a marked suppression of cell cycle progression that appears specific to the TIS state. In addition, we examined the expression of other genes linked to cell proliferation. Both TOP2A and MKI67 – markers typically associated with dividing cells – showed low expression in the TIS population, further supporting the idea that these cells are in a non-proliferative state (Figure 22A and B, top right and bottom left panels). Interestingly, a small group of TIS cells – termed 'escapers' –

displayed a mixed expression profile, characterized by the simultaneous presence of proliferation- and arrest-associated transcripts. These cells, marked within dotted regions on the UMAP plots, may represent a transitional subset capable of re-entering the cell cycle and giving rise to REPOP cells.

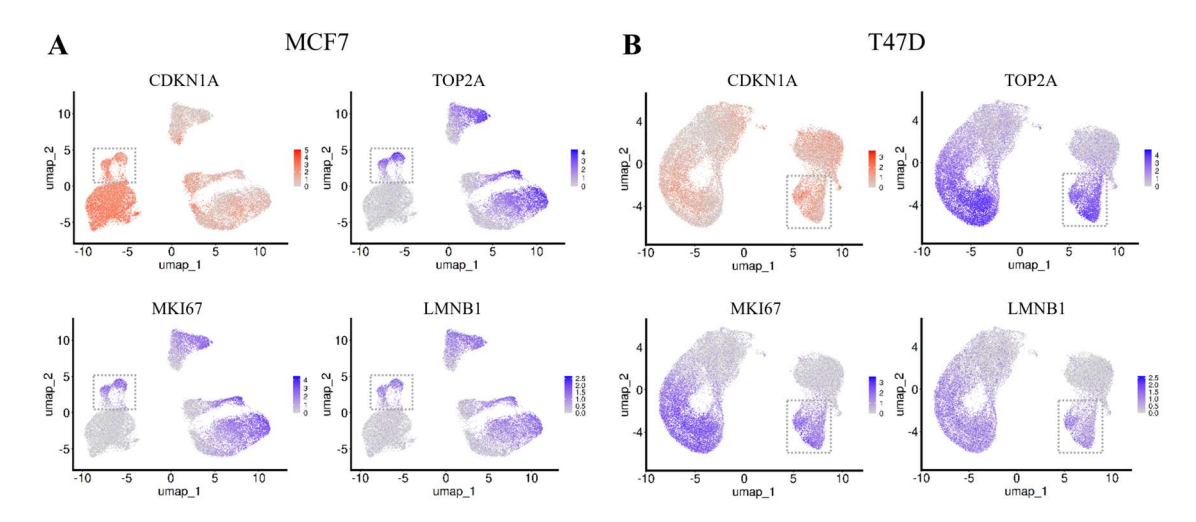
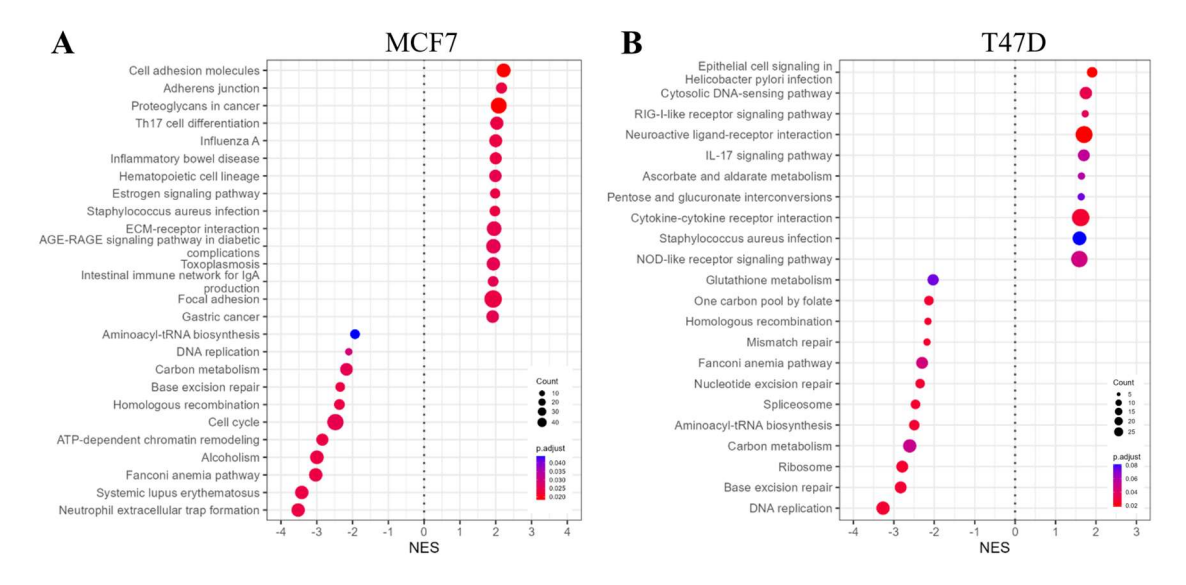


Figure 22. Feature plots showing expression patterns of TIS- and proliferation-associated genes in individual MCF7 (A) and T47D (B) cells. TIS populations exhibit strong CDKN1A (p21) expression, indicative of cell cycle arrest (top left panels). In contrast, genes typically linked to active proliferation – such as LMNB1, TOP2A, and MK167 – are downregulated (top right and bottom panels), consistent with the TIS state. A subset of TIS cells marked with dotted regions, referred to as 'escapers', shows elevated levels of these proliferation markers, suggesting the presence of a transcriptionally distinct group with potential to re-enter the cell cycle.

### 4.6.3. Pathway analysis

Single-cell transcriptomic analysis revealed characteristic molecular features of TIS cells that may underlie their survival and drug resistance. In MCF7 cells, several DNA repair pathways – including Homologous Recombination, Base Excision Repair, and the Fanconi Anemia Pathway – were markedly downregulated (Figure 23A), suggesting reduced genomic maintenance capacity. ATP-dependent chromatin remodeling and key regulators of the cell cycle and DNA replication were also suppressed, pointing to a stable growth-arrested state. In parallel, pathways related to Estrogen Signaling, ECM-receptor interactions, and Cell Adhesion Molecules were activated, possibly enhancing cell survival through microenvironmental interactions.

T47D cells showed a comparable transcriptional profile (Figure 23B), including downregulation of the same three DNA repair pathways observed in MCF7. Additionally, Mismatch Repair and Nucleotide Excision Repair pathways were also downregulated, indicating a more extensive reduction in genome maintenance capacity. Beyond DNA repair, decreased activity in the Spliceosome and the One-Carbon Pool by Folate pathway suggests disruption in RNA splicing and folate-mediated metabolic processes, which may further stabilize the senescent state. Altogether, these findings highlight coordinated pathway-level changes that support TIS cell persistence and resistance to therapy.



**Figure 23.** Gene set enrichment analysis (GSEA) was performed to compare gene expression profiles between MCF7 (A) and T47D (B) TIS and CTR cells. Normalized enrichment scores (NES) indicate the direction of pathway regulation, with positive scores indicating upregulated pathways and negative values indicating downregulated pathways.

### 4.6.4. Trajectory analysis of cell states

To explore transcriptomic transitions between cell states, trajectory analysis was performed on CTR, TIS, and REPOP populations (Figure 24A, B). A set of 93 genes found to be differentially expressed between CTR and TIS across both MCF7 and T47D lines were mapped along the trajectories. In MCF7 cells, TIS populations form a distinct cluster, while REPOP cells shift back toward CTR, indicating partial transcriptomic recovery. In T47D, REPOP and CTR cells show near-complete overlap, suggesting full exit from senescence and restoration of a proliferative state.

Trajectory mapping highlighted the reactivation of the cell cycle as a key feature of the TIS-to-REPOP transition. To rule out the possibility that this was driven solely by cell cycle genes, the analysis was repeated with these genes excluded. The outcome remained unchanged, supporting the conclusion that senescence is reversible and that TIS cells can resume proliferation once cell cycle arrest is terminated.

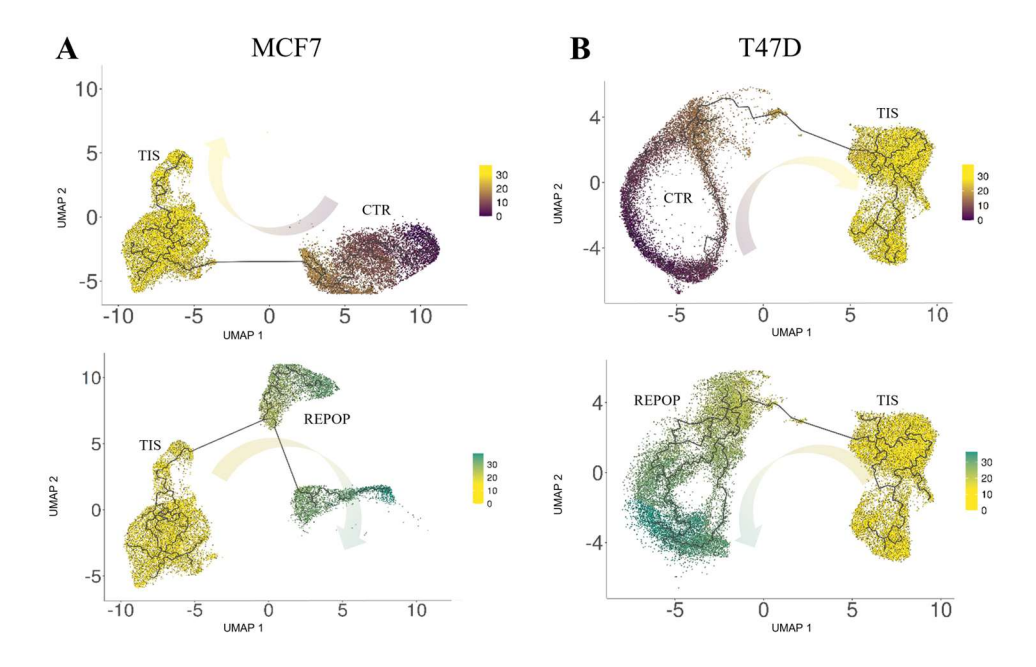


Figure 24. (A,B) UMAP trajectory analysis of MCF7 (A) and T47D (B) cells, showing changes in gene expression along transitions between different cellular states. The upper panels illustrate the shift from CTR to the TIS state, while the bottom panels trace the progression from TIS to REPOP.

### 4.6.5. Drug resistance analysis

To explore potential contributors to drug resistance in TIS cells, we analyzed the expression of selected resistance-related genes (Figure 25). No shared mechanism was identified across both cell lines. Although certain changes – such as decreased TOP2A in MCF7 or reduced NEDD8 in T47D – appeared potentially relevant, these associations were not observed in the other cell line or in REPOP states. Notably, both models remained resistant to topoisomerase II inhibitors and pevonedistat despite opposing expression trends. These observations, in line with bulk RNA-seq results, point toward a more complex, multifactorial basis for drug resistance in TIS cells that is unlikely to be explained by single-gene effects.

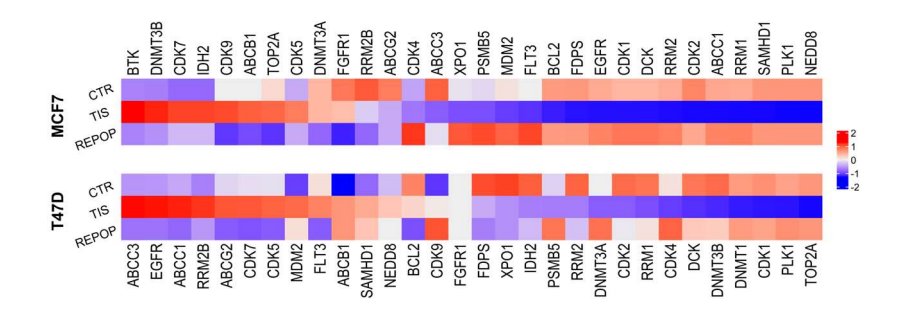
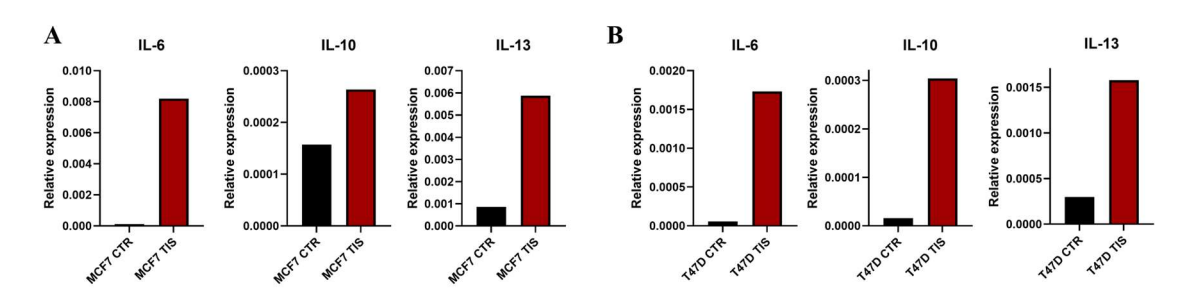


Figure 25. Heatmap showing expression of genes linked to drug resistance, senescence, and cell cycle control across CTR, TIS, and REPOP states in MCF7 and T47D cells. Senescence markers are upregulated in TIS and downregulated in REPOP, while drug resistance genes show variable expression patterns between the two models. The data illustrate the intricate relationship between senescence, proliferative capacity, and treatment response.

### 4.7. Investigation of the immunomodulatory effect of TIS cells

To determine whether TIS cells can modulate their immune environment, we analyzed cytokine mRNA expression levels in MCF7 and T47D cell lines (Figure 26), with a specialized assay performed by Károly Hegedűs. IL6 showed the most pronounced upregulation, with a 70-fold increase in MCF7 and a 32-fold increase in T47D cells. IL13 expression was also strongly upregulated, with 7-fold and 5-fold elevations in MCF7 and T47D, respectively. IL10 expression exhibited cell line-specific differences: while T47D TIS cells demonstrated a striking 19-fold increase, the elevation in MCF7 was modest (1.7-fold).



**Figure 26.** Cytokine expression profiling of CTR and TIS cells derived from **(A)** MCF7 and **(B)** T47D cultures. Relative expression levels of 3 immunosuppressive cytokines. Cytokine expression data were normalized to the average cycle threshold (Ct) of the four reference genes to ensure accurate quantification.

These cytokines are known to contribute to immune evasion and tumor-promoting processes: IL6 promotes the accumulation of myeloid-derived suppressor cells, which reduce T-cell-mediated antitumor responses (82), IL10 decreases immune activity and supports angiogenesis (83), and IL13 leads to macrophage polarization toward an immunosuppressive, tumor-supportive state (84). Together, these changes may alter the tumor microenvironment by reducing immune surveillance and creating conditions that support tumor development.

### 4.8. Surface proteomic profiling of TIS

To identify potential therapeutic targets specific to senescent cancer cells, we analyzed surface and secreted proteins with potential relevance for immunotherapy or targeted inhibition. The proteomic experiments and data analyses were carried out by Gábor Tusnády and Tamás Langó, using a biotin-based labeling method optimized for capturing membrane-bound and secreted proteins, as developed by Langó et al. (66, 85). This method was applied to MCF7 CTR, TIS and REPOP cells. Clustering analysis based on 6 CTR, 8 TIS, and 8 REPOP replicates showed that TIS cells segregated clearly from both CTR and REPOP groups, which exhibited similar protein expression profiles (Figure 27).

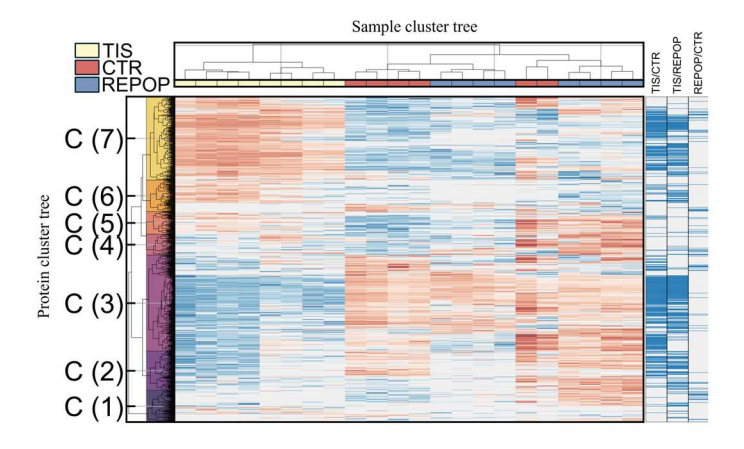
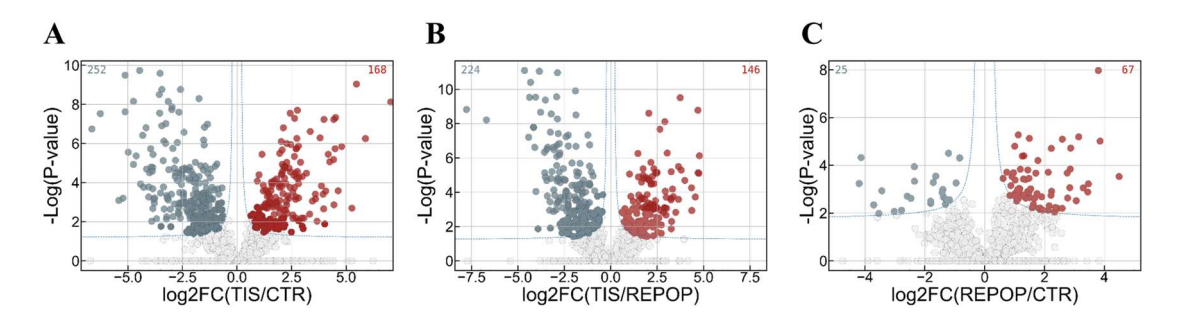


Figure 27. Hierarchical clustering of proteomic profiles (Z-score normalized) from MCF7 CTR, TIS, and REPOP conditions. Euclidean distances were calculated between data points in both the sample (columns) and protein (rows) dimensions, and clustering was performed accordingly. TIS samples (yellow) form a distinct cluster, clearly separated from CTR (red) and REPOP (blue) samples. Several protein clusters (C1–C7) exhibit coordinated upregulation (red) or downregulation (blue) across sample groups. Statistically significant proteins (FDR < 0.05) are marked on the right.

When comparing TIS cells to CTR and REPOP states, 420 proteins were differentially expressed between CTR and TIS, and 370 between TIS and REPOP, while only 92 proteins differed between CTR and REPOP (Figure 28). These findings support our previous results, indicating that TIS is characterized by a distinct, yet reversible, shift in the surface proteome.



**Figure 28.** Volcano plots displaying differentially expressed proteins during the transitions from CTR to TIS (A), TIS to REPOP (B), and CTR to REPOP (C). Significantly altered proteins (FDR<0.05) are highlighted in red (upregulated) or blue (downregulated), with thresholds marked by blue dotted lines. The number of significant changes is indicated in the top corners of each panel.

Proteomic analysis identified 95 proteins that were specifically overexpressed in TIS cells, underscoring the distinct molecular features of the senescent state (Figure 29).

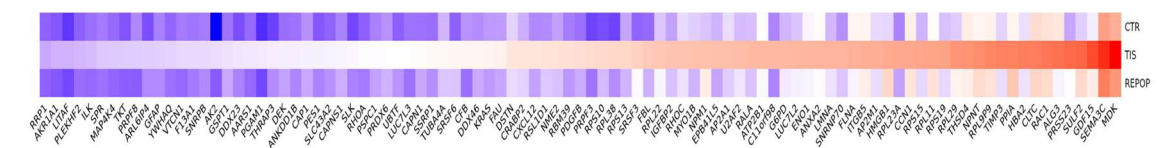


**Figure 29.** Heatmap showing 95 proteins selectively upregulated in TIS cells, highlighting the unique proteomic profile associated with the senescent state.

Of these, 41 had previously been associated with cellular senescence, and 17 were linked to alternative splicing and spliceosome. Several proteins – FBL (86), NME2 (87), FLNA (88), ENO1 (89), and ANXA2 (90) – have also been identified as SASP components in senescent fibroblasts induced by irradiation, oncogenic RAS, or atazanavir treatment, highlighting similarities between TIS and senescence observed in non-malignant cells.

We also detected plasma membrane localization of HMGB1, a damage-associated molecular pattern (DAMP) molecule known to translocate from the nucleus during senescence (91, 92), as well as secretion of GDF15, an emerging marker of aging and

senescence (93). The enrichment of spliceosome-related proteins suggests that RNA splicing may contribute to the establishment or maintenance of the senescent state. The remaining 52 proteins have not been previously linked to senescence and may represent novel regulators or biomarkers of the TIS state.

Additionally, our proteomic analysis identified a cell surface protein that was exclusively expressed on senescent cells. Given its apparent specificity for the senescent state, this protein may serve as a promising immunotherapeutic target for the selective elimination of TIS cells, with minimal impact on non-senescent populations. The exploitability of this marker is currently being evaluated in collaboration with several research groups. As prior art searches and intellectual property assessments are ongoing, the precise identity of the protein is not disclosed at this stage.

#### 5. Discussion

Therapy-induced senescence (TIS) TIS has been considered a beneficial outcome of cancer treatment, as it stops tumor cells from proliferating without necessarily causing cell death (40). This strategy aims to halt tumor cell proliferation by inducing permanent growth arrest, thereby reducing the need for high-dose cytotoxic treatments, which are often associated with toxicity and the development of resistance (94). However, our findings suggest that TIS may represent a transient, drug-tolerant state rather than a stable endpoint, raising concerns about its long-term therapeutic value and highlighting the need to re-evaluate its role in cancer therapy.

To effectively compare findings across studies, a clear definition of TIS is crucial, yet a major challenge remains the lack of a universal marker for identifying senescent cells. No single biomarker can definitively establish senescence, therefore, using a combination of multiple markers is necessary for reliable identification of senescent cells (43, 44). In addition, Ashraf et al. demonstrated that even the presence of multiple markers does not guarantee that a cell is truly senescent (95).

Our results strongly supported the presence of TIS in the surviving cell populations. In addition to classical senescence markers such morphology, X-Gal staining, CDKN1A and LMNB1, both transcriptomic and proteomic analyses revealed TIS-associated features. In addition to well-known senescence markers such as upregulation of CDKN1A and downregulation of LMNB1, our transcriptomic analysis revealed a unique gene expression profile that was consistently upregulated during TIS across all examined breast cancer cell lines, suggesting the presence of a potential TIS-specific signature. This included genes linked to senescence (e.g., MMP12 (96), CYP1A1 (97), BIRC3 (98), COL4A3 (99), NTRK2 (100) and aging (e.g., CCL26 (101), GRID2 (102), CA10 (103), CLEC12A (104). Proteomic profiling of the surfaceome showed increased secretion of various components, including SASP-related proteins, translocated HMGB1, and ribosomal elements. This reproducible pattern suggests the existence of a TIS-specific molecular profile that may serve as a potential biomarker set for identifying senescent cells in breast cancer.

A growing number of studies indicate that TIS cells can eventually escape this state; however, the duration of the inducing treatment plays a critical role in this context. Senescence is generally considered irreversible when the stimulus persists for more than

4 days (105, 106). However, if the treatment lasts less than 96 hours, many cancer cells retain the ability to evade senescence and later resume proliferation. In early studies, Robertson et al. showed that a small fraction of non-small cell lung cancer cells – lacking both p16 and p53, which are known to limit senescence reversibility – escaped therapyinduced senescence after 1-3 days of camptothecin treatment, with proliferative outgrowth observed within 20-25 days (41). Saleh et al. conducted a series of studies on TIS escape across various cancer cell lines, using treatments of less than 24 hours. In most cases, the cells resumed proliferation within 5 to 7 days after drug removal (42, 63). Ashraf et al. induced senescence by treating cells with etoposide for 24 hours; however, approximately 1.7% of the cells escaped growth arrest and resumed proliferation within 10 days (95).

In contrast to previous studies, we used a significantly longer drug exposure (120 hours), followed by analysis of surviving cells 12 days after the initial treatment to ensure that senescence was fully established. In our system, repopulation occurred only after more than 25 days, closely resembling relapse dynamics observed in a clinically relevant mouse model of triple-negative breast cancer treated with doxorubicin (107, 108). Given these complexities, our approach prioritized not only the detection of senescence markers but also functional validation to accurately characterize the TIS phenotype.

In addition to examining the phenomenon of TIS escape, our study aimed to characterize the defining features of the REPOP state. Although REPOP cells closely resemble CTR cells in drug sensitivity and gene expression, transcriptomic analysis revealed a 23-gene signature that persisted from the TIS state. Among these, IFIT1 was consistently upregulated in all four cell lines, while 22 other genes showed persistent expression in at least three cell lines. IFIT1 has been previously linked to residual breast cancer and has been identified as part of an interferon-related DNA damage resistance signature alongside ISG15 (109, 110). Among the 22 genes, additional IFIT family members such as IFIT3 and IFITM1 were also identified. IFIT3 has been linked to senescence regulation and poor therapy response in various cancers (111, 112), while IFITM1 is associated with treatment resistance and immune evasion (113, 114). These genes stayed overexpressed even after cells escaped senescence, suggesting that TIS leaves a lasting molecular mark, that may help the repopulating cancer cells survive, avoid the immune system, and resist later treatments.

Senolytic agents offer potential for eliminating senescent cells and thereby preventing their detrimental effects. Among these, antiapoptotic Bcl-2 inhibitors were developed to target the apoptosis-resistant phenotype characteristic of senescent cells. Although earlier studies reported that Bcl-2 inhibitors efficiently target senescent cells (59-61), our results did not fully support these findings. Venetoclax showed similar toxicity in CTR and TIS cells, and although navitoclax, ABT-737, and A1331852 showed some TIS-selective activity *in vitro*, the long-term efficacy of navitoclax was inconsistent and showed no significant impact *in vivo*. Importantly, in our experiments, neither the expression levels of Bcl-2 and Bcl-XL nor their subcellular distribution correlated with drug sensitivity. These observations suggest that the effects of these compounds may be mediated by alternative mechanisms rather than direct targeting of Bcl-2/xL in TIS cells.

Moreover, the apoptosis-resistant phenotype would also imply a broader drug resistance in TIS cells, which was not consistently supported by our data. In our experiments, HDAC inhibitors – despite their proposed senolytic and apoptosis-inducing potential (115, 116) – exhibited similar toxicity in both CTR and TIS cells. Likewise, proteasome and tyrosine kinase inhibitors, known to trigger apoptosis, did not show resistance in TIS cells (117, 118). These observations do not support the notion that TIS cancer cells are generally resistant to apoptosis.

Although a defining feature of senescent cells is their lack of proliferation, which is typically associated with increased tolerance to chemotherapy (119), our results indicate a more complex relationship between TIS and drug sensitivity. Proliferation-dependent drugs such as AT7519 (120), ibrutinib (121), masitinib, sorafenib and sunitinib (122) effectively eliminated TIS cells, despite their non-proliferate state. In contrast, drugs known to target non-dividing cells, like carfilzomib (123), homoharringtonine (124), and melphalan (125), showed no effect. This paradox suggests that the chemoresistance observed in TIS is not solely due to cell cycle arrest but involves distinct, non-canonical protective mechanisms (126).

In our study, we detected several spliceosome-related proteins among the secreted surfaceome components. While the role of the spliceosome in cellular senescence (127, 128) and SASP (129) is still being uncovered, its contribution to intercellular communication remains unclear. Under stress conditions – such as chemotherapy or hypoxia – key splicing factors like SRSF1 and SRSF3 are known to shift from the nucleus

to the cytoplasm and may be released via extracellular vesicles (130). This mechanism could influence neighboring cells by modulating their stress response capacity. Our findings support the hypothesis that secreted spliceosome proteins could contribute to adaptive responses during TIS.

Previous studies indicate that TIS cells play a dual role in immune regulation. On one hand, they can trigger immune-mediated tumor suppression – a process referred to as "senescence surveillance" – while on the other, they may facilitate immune evasion and support tumor progression (21, 27, 28). Also some studies report that senescent cells are immunogenic and subject to immune clearance (131, 132), others suggest they can escape immune detection (133, 134). In our experiments, TIS cells showed marked changes in signaling pathways related to immune and environmental interactions and support the notion of an immune-evasive phenotype. The modulation of Cytokine-Cytokine Receptor Interaction pathway and activation of Neuroactive Ligand-Receptor Interaction pathways suggest an altered communication profile that may promote immune evasion and longterm persistence. Furthermore, activation of Cytosolic DNA-Sensing Pathway and Helicobacter pylori and Staphylococcus aureus Infection pathways points to adaptive responses that help TIS cells cope with chronic inflammation or microbial stress. Several overexpressed genes in TIS cells, including LGALS9 (135), CXCL12 (136), TREM1 (137), and MACC1 (138), have previously been implicated in suppressing T cell activity or promoting immune escape. The observed upregulation of IL6, IL10, and IL13 cytokines in TIS cells suggests that TIS may actively contribute to remodeling the tumor microenvironment. These cytokines are associated with immunosuppressive mechanisms, such as reduced T-cell activity (82), enhanced accumulation of suppressive immune cells (82), and macrophage polarization (84). In line with previous findings by Ruhland et al., IL6 may promote a pro-tumorigenic niche and sustaining chronic inflammation (29). Moreover, IL6 has been implicated in angiogenesis, further supporting tumor progression and survival (27). These findings point to a complex immunosuppressive phenotype in TIS cells that may support their long-term persistence and present challenges for immune-mediated clearance.

#### 6. Conclusions

- High-dose doxorubicin treatment successfully induced therapy-induced senescence (TIS) in four breast cancer cell lines, as confirmed by a multimarker analysis of senescence-associated characteristics.
- ❖ Our findings demonstrate that TIS is a reversible state. All examined cell lines escaped TIS over time and formed repopulating (REPOP) cells with control-like morphology and transcriptional profile. After repeated treatment, REPOP cells rentered senescence and re-established resistance, confirming TIS reversibility.
- Senolytic agents showed limited efficacy against TIS cells. While some Bcl-2/Bcl-XL inhibitors had partial effects *in vitro*, the long-term effect of navitoclax was inconsistent, and no significant difference in tumor relapse time was observed *in vivo*.
- ❖ Our drug screening studies revealed that TIS cells have a unique resistance profile with broad resistance to multiple chemotherapeutic agents. This phenotype was absent in control (CTR) and REPOP cells but reappeared in re-TIS cells. Resistance was not explained by classical mechanisms, suggesting involvement of non-canonical regulatory processes.
- ❖ Bulk and single-cell RNA sequencing revealed extensive transcriptional reprogramming in TIS cells, including the downregulation of proliferation and DNA repair pathways and the modulation of immune-related signaling. These changes were reversed in REPOP cells, highlighting the dynamic nature of the TIS state. Single-cell analyses also highlighted the heterogeneity of REPOP populations and suggested the presence of a distinct subset of 'escaper' cells that may drive repopulation after senescence.
- Proteomic profiling of surface-expressed and secreted proteins identified 95 proteins uniquely upregulated in TIS. This included known senescence markers and SASP factors, as well as novel candidates related to splicing and immune modulation. These findings could contribute to the identification of TIS-related biomarkers.

### 7. Summary

Our study provides a detailed characterization of therapy-induced senescence (TIS) in breast cancer, revealing it as a dynamic and reversible cell state. Using optimized in vitro models and multiple molecular approaches – including bulk and single-cell RNA sequencing and surface proteomics – we demonstrated that TIS is not a terminal growth arrest, but rather a transitional state associated with distinct molecular and phenotypic changes.

TIS cells showed resistance to a wide range of chemotherapeutics, including commonly used drugs in breast cancer treatment, yet this resistance was reversible upon exit from senescence, indicating that TIS alone temporarily protects cancer cells from treatment. Despite extensive molecular profiling, no single resistance gene or canonical pathway could explain the observed drug tolerance, suggesting that TIS-associated resistance arises from multifactorial, context-dependent processes. The limited response of TIS cells to senolytic agents further highlights their therapeutic challenge, as our results were inconsistent across different compounds and conditions.

Whereas TIS is often viewed as a beneficial endpoint that halts tumor progression, our results show that TIS cells can re-enter the cell cycle and repopulate cultures, accompanied by transcriptional reversal. Transcriptomic analyses revealed widespread gene expression changes during TIS, characterized by downregulation of proliferation and DNA repair pathways and modulation of immune-related programs. Notably, these changes were reversed in repopulating cells, highlighting the plasticity of this state. Importantly, TIS cells exhibited immune-evasive features, including altered immune signaling and increased expression of immunosuppressive factors, potentially enabling them to escape immune clearance and persist over time, further complicating therapeutic elimination.

In conclusion, this work redefines TIS as a reversible, adaptive resistance phenotype in breast cancer, highlighting the limitations of TIS as a therapeutic endpoint. It also underscores the challenges of targeting TIS cells with current agents and emphasizes the need for novel treatment strategies. Further research will be needed to uncover regulatory mechanisms – such as chromatin remodeling, RNA processing, epigenomic regulation and immune evasion – that sustain the TIS state and enable its reversal, with the goal of preventing relapse and improving long-term treatment outcomes.

#### 8. References

- 1. Bray F, Laversanne M, Sung H, Ferlay J, Siegel RL, Soerjomataram I, Jemal A. Global cancer statistics 2022: GLOBOCAN estimates of incidence and mortality worldwide for 36 cancers in 185 countries. CA Cancer J Clin. 2024;74(3):229-63.
- 2. Mansoori B, Mohammadi A, Davudian S, Shirjang S, Baradaran B. The Different Mechanisms of Cancer Drug Resistance: A Brief Review. Adv Pharm Bull. 2017;7(3):339-48.
- 3. Longley DB, Johnston PG. Molecular mechanisms of drug resistance. J Pathol. 2005;205(2):275-92.
- 4. Wang X, Zhang H, Chen X. Drug resistance and combating drug resistance in cancer. Cancer Drug Resist. 2019;2(2):141-60.
- 5. Noll EM, Eisen C, Stenzinger A, Espinet E, Muckenhuber A, Klein C, Vogel V, Klaus B, Nadler W, Rosli C, Lutz C, Kulke M, Engelhardt J, Zickgraf FM, Espinosa O, Schlesner M, Jiang X, Kopp-Schneider A, Neuhaus P, Bahra M, Sinn BV, Eils R, Giese NA, Hackert T, Strobel O, Werner J, Buchler MW, Weichert W, Trumpp A, Sprick MR. CYP3A5 mediates basal and acquired therapy resistance in different subtypes of pancreatic ductal adenocarcinoma. Nat Med. 2016;22(3):278-87.
- 6. Christie EL, Pattnaik S, Beach J, Copeland A, Rashoo N, Fereday S, Hendley J, Alsop K, Brady SL, Lamb G, Pandey A, deFazio A, Thorne H, Bild A, Bowtell DDL. Multiple ABCB1 transcriptional fusions in drug resistant high-grade serous ovarian and breast cancer. Nat Commun. 2019;10(1):1295.
- 7. Helleday T, Petermann E, Lundin C, Hodgson B, Sharma RA. DNA repair pathways as targets for cancer therapy. Nat Rev Cancer. 2008;8(3):193-204.
- 8. Sugimoto Y, Tsukahara S, Oh-hara T, Isoe T, Tsuruo T. Decreased expression of DNA topoisomerase I in camptothecin-resistant tumor cell lines as determined by a monoclonal antibody. Cancer Res. 1990;50(21):6925-30.
- 9. Kuroda J, Puthalakath H, Cragg MS, Kelly PN, Bouillet P, Huang DC, Kimura S, Ottmann OG, Druker BJ, Villunger A, Roberts AW, Strasser A. Bim and Bad mediate imatinib-induced killing of Bcr/Abl+ leukemic cells, and resistance due to their loss is overcome by a BH3 mimetic. Proc Natl Acad Sci U S A. 2006;103(40):14907-12.
- 10. Shah MA, Schwartz GK. Cell cycle-mediated drug resistance: an emerging concept in cancer therapy. Clin Cancer Res. 2001;7(8):2168-81.

- 11. Vajda F, Bajtai E, Gombos B, Karai E, Hamori L, Szakacs G, Furedi A. [Development of novel treatment strategies for drug resistant cancer]. Magy Onkol. 2021;65(2):176-87.
- 12. Zhu X, Tian T, Ruan M, Rao J, Yang W, Cai X, Sun M, Qin G, Zhao Z, Wu J, Shao Z, Shui R, Hu Z. Expression of DNA Damage Response Proteins and Associations with Clinicopathologic Characteristics in Chinese Familial Breast Cancer Patients with BRCA1/2 Mutations. J Breast Cancer. 2018;21(3):297-305.
- 13. Ganapathi RN, Ganapathi MK. Mechanisms regulating resistance to inhibitors of topoisomerase II. Front Pharmacol. 2013;4:89.
- 14. Motwani M, Delohery TM, Schwartz GK. Sequential dependent enhancement of caspase activation and apoptosis by flavopiridol on paclitaxel-treated human gastric and breast cancer cells. Clin Cancer Res. 1999;5(7):1876-83.
- 15. Matt S, Hofmann TG. The DNA damage-induced cell death response: a roadmap to kill cancer cells. Cell Mol Life Sci. 2016;73(15):2829-50.
- 16. Hayflick L, Moorhead PS. The serial cultivation of human diploid cell strains. Exp Cell Res. 1961;25:585-621.
- 17. Coppe JP, Desprez PY, Krtolica A, Campisi J. The senescence-associated secretory phenotype: the dark side of tumor suppression. Annu Rev Pathol. 2010;5:99-118.
- 18. Demaria M, Ohtani N, Youssef SA, Rodier F, Toussaint W, Mitchell JR, Laberge RM, Vijg J, Van Steeg H, Dolle ME, Hoeijmakers JH, de Bruin A, Hara E, Campisi J. An essential role for senescent cells in optimal wound healing through secretion of PDGF-AA. Dev Cell. 2014;31(6):722-33.
- 19. Storer M, Mas A, Robert-Moreno A, Pecoraro M, Ortells MC, Di Giacomo V, Yosef R, Pilpel N, Krizhanovsky V, Sharpe J, Keyes WM. Senescence is a developmental mechanism that contributes to embryonic growth and patterning. Cell. 2013;155(5):1119-30.
- 20. Munoz-Espin D, Canamero M, Maraver A, Gomez-Lopez G, Contreras J, Murillo-Cuesta S, Rodriguez-Baeza A, Varela-Nieto I, Ruberte J, Collado M, Serrano M. Programmed cell senescence during mammalian embryonic development. Cell. 2013;155(5):1104-18.

- 21. Kang TW, Yevsa T, Woller N, Hoenicke L, Wuestefeld T, Dauch D, Hohmeyer A, Gereke M, Rudalska R, Potapova A, Iken M, Vucur M, Weiss S, Heikenwalder M, Khan S, Gil J, Bruder D, Manns M, Schirmacher P, Tacke F, Ott M, Luedde T, Longerich T, Kubicka S, Zender L. Senescence surveillance of pre-malignant hepatocytes limits liver cancer development. Nature. 2011;479(7374):547-51.
- 22. Nelson G, Wordsworth J, Wang C, Jurk D, Lawless C, Martin-Ruiz C, von Zglinicki T. A senescent cell bystander effect: senescence-induced senescence. Aging Cell. 2012;11(2):345-9.
- 23. Acosta JC, Banito A, Wuestefeld T, Georgilis A, Janich P, Morton JP, Athineos D, Kang TW, Lasitschka F, Andrulis M, Pascual G, Morris KJ, Khan S, Jin H, Dharmalingam G, Snijders AP, Carroll T, Capper D, Pritchard C, Inman GJ, Longerich T, Sansom OJ, Benitah SA, Zender L, Gil J. A complex secretory program orchestrated by the inflammasome controls paracrine senescence. Nat Cell Biol. 2013;15(8):978-90.
- 24. Armanios M, Alder JK, Parry EM, Karim B, Strong MA, Greider CW. Short telomeres are sufficient to cause the degenerative defects associated with aging. Am J Hum Genet. 2009;85(6):823-32.
- 25. Wang C, Jurk D, Maddick M, Nelson G, Martin-Ruiz C, von Zglinicki T. DNA damage response and cellular senescence in tissues of aging mice. Aging Cell. 2009;8(3):311-23.
- 26. Lopez-Otin C, Blasco MA, Partridge L, Serrano M, Kroemer G. The hallmarks of aging. Cell. 2013;153(6):1194-217.
- 27. Ancrile B, Lim KH, Counter CM. Oncogenic Ras-induced secretion of IL6 is required for tumorigenesis. Genes Dev. 2007;21(14):1714-9.
- 28. Ortiz-Montero P, Londono-Vallejo A, Vernot JP. Senescence-associated IL-6 and IL-8 cytokines induce a self- and cross-reinforced senescence/inflammatory milieu strengthening tumorigenic capabilities in the MCF-7 breast cancer cell line. Cell Commun Signal. 2017;15(1):17.
- 29. Ruhland MK, Loza AJ, Capietto AH, Luo X, Knolhoff BL, Flanagan KC, Belt BA, Alspach E, Leahy K, Luo J, Schaffer A, Edwards JR, Longmore G, Faccio R, DeNardo DG, Stewart SA. Stromal senescence establishes an immunosuppressive microenvironment that drives tumorigenesis. Nat Commun. 2016;7:11762.

- 30. Eggert T, Wolter K, Ji J, Ma C, Yevsa T, Klotz S, Medina-Echeverz J, Longerich T, Forgues M, Reisinger F, Heikenwalder M, Wang XW, Zender L, Greten TF. Distinct Functions of Senescence-Associated Immune Responses in Liver Tumor Surveillance and Tumor Progression. Cancer Cell. 2016;30(4):533-47.
- 31. Coppe JP, Patil CK, Rodier F, Sun Y, Munoz DP, Goldstein J, Nelson PS, Desprez PY, Campisi J. Senescence-associated secretory phenotypes reveal cell-nonautonomous functions of oncogenic RAS and the p53 tumor suppressor. PLoS Biol. 2008;6(12):2853-68.
- 32. Cahu J, Bustany S, Sola B. Senescence-associated secretory phenotype favors the emergence of cancer stem-like cells. Cell Death Dis. 2012;3(12):e446.
- 33. Schumacher B, Pothof J, Vijg J, Hoeijmakers JHJ. The central role of DNA damage in the ageing process. Nature. 2021;592(7856):695-703.
- 34. Huang W, Hickson LJ, Eirin A, Kirkland JL, Lerman LO. Cellular senescence: the good, the bad and the unknown. Nat Rev Nephrol. 2022;18(10):611-27.
- 35. Serrano M, Lin AW, McCurrach ME, Beach D, Lowe SW. Oncogenic ras provokes premature cell senescence associated with accumulation of p53 and p16INK4a. Cell. 1997;88(5):593-602.
- 36. Wang X, Wong SC, Pan J, Tsao SW, Fung KH, Kwong DL, Sham JS, Nicholls JM. Evidence of cisplatin-induced senescent-like growth arrest in nasopharyngeal carcinoma cells. Cancer Res. 1998;58(22):5019-22.
- 37. Chang BD, Broude EV, Dokmanovic M, Zhu H, Ruth A, Xuan Y, Kandel ES, Lausch E, Christov K, Roninson IB. A senescence-like phenotype distinguishes tumor cells that undergo terminal proliferation arrest after exposure to anticancer agents. Cancer Res. 1999;59(15):3761-7.
- 38. te Poele RH, Okorokov AL, Jardine L, Cummings J, Joel SP. DNA damage is able to induce senescence in tumor cells in vitro and in vivo. Cancer Res. 2002;62(6):1876-83.
- 39. Sidi R, Pasello G, Opitz I, Soltermann A, Tutic M, Rehrauer H, Weder W, Stahel RA, Felley-Bosco E. Induction of senescence markers after neo-adjuvant chemotherapy of malignant pleural mesothelioma and association with clinical outcome: an exploratory analysis. Eur J Cancer. 2011;47(2):326-32.

- 40. Nardella C, Clohessy JG, Alimonti A, Pandolfi PP. Pro-senescence therapy for cancer treatment. Nat Rev Cancer. 2011;11(7):503-11.
- 41. Roberson RS, Kussick SJ, Vallieres E, Chen SY, Wu DY. Escape from therapy-induced accelerated cellular senescence in p53-null lung cancer cells and in human lung cancers. Cancer Res. 2005;65(7):2795-803.
- 42. Saleh T, Tyutyunyk-Massey L, Murray GF, Alotaibi MR, Kawale AS, Elsayed Z, Henderson SC, Yakovlev V, Elmore LW, Toor A, Harada H, Reed J, Landry JW, Gewirtz DA. Tumor cell escape from therapy-induced senescence. Biochem Pharmacol. 2019;162:202-12.
- 43. Hernandez-Segura A, Nehme J, Demaria M. Hallmarks of Cellular Senescence. Trends Cell Biol. 2018;28(6):436-53.
- 44. Gorgoulis V, Adams PD, Alimonti A, Bennett DC, Bischof O, Bishop C, Campisi J, Collado M, Evangelou K, Ferbeyre G, Gil J, Hara E, Krizhanovsky V, Jurk D, Maier AB, Narita M, Niedernhofer L, Passos JF, Robbins PD, Schmitt CA, Sedivy J, Vougas K, von Zglinicki T, Zhou D, Serrano M, Demaria M. Cellular Senescence: Defining a Path Forward. Cell. 2019;179(4):813-27.
- 45. Hayflick L. The Limited in Vitro Lifetime of Human Diploid Cell Strains. Exp Cell Res. 1965;37:614-36.
- 46. Freund A, Laberge RM, Demaria M, Campisi J. Lamin B1 loss is a senescence-associated biomarker. Mol Biol Cell. 2012;23(11):2066-75.
- 47. Beausejour CM, Krtolica A, Galimi F, Narita M, Lowe SW, Yaswen P, Campisi J. Reversal of human cellular senescence: roles of the p53 and p16 pathways. EMBO J. 2003;22(16):4212-22.
- 48. Lawless C, Wang C, Jurk D, Merz A, Zglinicki T, Passos JF. Quantitative assessment of markers for cell senescence. Exp Gerontol. 2010;45(10):772-8.
- 49. Dimri GP, Lee X, Basile G, Acosta M, Scott G, Roskelley C, Medrano EE, Linskens M, Rubelj I, Pereira-Smith O, et al. A biomarker that identifies senescent human cells in culture and in aging skin in vivo. Proc Natl Acad Sci U S A. 1995;92(20):9363-7.
- 50. Severino J, Allen RG, Balin S, Balin A, Cristofalo VJ. Is beta-galactosidase staining a marker of senescence in vitro and in vivo? Exp Cell Res. 2000;257(1):162-71.

- 51. Krizhanovsky V, Xue W, Zender L, Yon M, Hernando E, Lowe SW. Implications of cellular senescence in tissue damage response, tumor suppression, and stem cell biology. Cold Spring Harb Symp Quant Biol. 2008;73:513-22.
- 52. Franceschi C, Campisi J. Chronic inflammation (inflammaging) and its potential contribution to age-associated diseases. J Gerontol A Biol Sci Med Sci. 2014;69 Suppl 1:S4-9.
- 53. Gonzalez-Gualda E, Baker AG, Fruk L, Munoz-Espin D. A guide to assessing cellular senescence in vitro and in vivo. FEBS J. 2021;288(1):56-80.
- 54. Zhang L, Pitcher LE, Prahalad V, Niedernhofer LJ, Robbins PD. Targeting cellular senescence with senotherapeutics: senolytics and senomorphics. FEBS J. 2023;290(5):1362-83.
- 55. Selvarani R, Mohammed S, Richardson A. Effect of rapamycin on aging and agerelated diseases-past and future. Geroscience. 2021;43(3):1135-58.
- 56. Zhu Y, Tchkonia T, Pirtskhalava T, Gower AC, Ding H, Giorgadze N, Palmer AK, Ikeno Y, Hubbard GB, Lenburg M, O'Hara SP, LaRusso NF, Miller JD, Roos CM, Verzosa GC, LeBrasseur NK, Wren JD, Farr JN, Khosla S, Stout MB, McGowan SJ, Fuhrmann-Stroissnigg H, Gurkar AU, Zhao J, Colangelo D, Dorronsoro A, Ling YY, Barghouthy AS, Navarro DC, Sano T, Robbins PD, Niedernhofer LJ, Kirkland JL. The Achilles' heel of senescent cells: from transcriptome to senolytic drugs. Aging Cell. 2015;14(4):644-58.
- 57. Wang Y, Chang J, Liu X, Zhang X, Zhang S, Zhang X, Zhou D, Zheng G. Discovery of piperlongumine as a potential novel lead for the development of senolytic agents. Aging (Albany NY). 2016;8(11):2915-26.
- 58. Yousefzadeh MJ, Zhu Y, McGowan SJ, Angelini L, Fuhrmann-Stroissnigg H, Xu M, Ling YY, Melos KI, Pirtskhalava T, Inman CL, McGuckian C, Wade EA, Kato JI, Grassi D, Wentworth M, Burd CE, Arriaga EA, Ladiges WL, Tchkonia T, Kirkland JL, Robbins PD, Niedernhofer LJ. Fisetin is a senotherapeutic that extends health and lifespan. EBioMedicine. 2018;36:18-28.
- 59. Chang J, Wang Y, Shao L, Laberge RM, Demaria M, Campisi J, Janakiraman K, Sharpless NE, Ding S, Feng W, Luo Y, Wang X, Aykin-Burns N, Krager K, Ponnappan U, Hauer-Jensen M, Meng A, Zhou D. Clearance of senescent cells by ABT263 rejuvenates aged hematopoietic stem cells in mice. Nat Med. 2016;22(1):78-83.

- 60. Wang L, Doherty GA, Judd AS, Tao ZF, Hansen TM, Frey RR, Song X, Bruncko M, Kunzer AR, Wang X, Wendt MD, Flygare JA, Catron ND, Judge RA, Park CH, Shekhar S, Phillips DC, Nimmer P, Smith ML, Tahir SK, Xiao Y, Xue J, Zhang H, Le PN, Mitten MJ, Boghaert ER, Gao W, Kovar P, Choo EF, Diaz D, Fairbrother WJ, Elmore SW, Sampath D, Leverson JD, Souers AJ. Discovery of A-1331852, a First-in-Class, Potent, and Orally-Bioavailable BCL-X(L) Inhibitor. ACS Med Chem Lett. 2020;11(10):1829-36.
- 61. Yosef R, Pilpel N, Tokarsky-Amiel R, Biran A, Ovadya Y, Cohen S, Vadai E, Dassa L, Shahar E, Condiotti R, Ben-Porath I, Krizhanovsky V. Directed elimination of senescent cells by inhibition of BCL-W and BCL-XL. Nat Commun. 2016;7:11190.
- 62. Lamming DW, Ye L, Katajisto P, Goncalves MD, Saitoh M, Stevens DM, Davis JG, Salmon AB, Richardson A, Ahima RS, Guertin DA, Sabatini DM, Baur JA. Rapamycin-induced insulin resistance is mediated by mTORC2 loss and uncoupled from longevity. Science. 2012;335(6076):1638-43.
- 63. Saleh T, Cudjoe EK, Kyte SL, Henderson SC, Elmore LW, Gewirtz DA. Reversibility of chemotherapy-induced senescence is independent of autophagy and a potential model for tumor dormancy and cancer recurrence. bioRxiv. 2017:099812.
- 64. Milanovic M, Fan DNY, Belenki D, Dabritz JHM, Zhao Z, Yu Y, Dorr JR, Dimitrova L, Lenze D, Monteiro Barbosa IA, Mendoza-Parra MA, Kanashova T, Metzner M, Pardon K, Reimann M, Trumpp A, Dorken B, Zuber J, Gronemeyer H, Hummel M, Dittmar G, Lee S, Schmitt CA. Senescence-associated reprogramming promotes cancer stemness. Nature. 2018;553(7686):96-100.
- 65. Yang L, Fang J, Chen J. Tumor cell senescence response produces aggressive variants. Cell Death Discov. 2017;3:17049.
- 66. Lango T, Kuffa K, Toth G, Turiak L, Drahos L, Tusnady GE. Comprehensive Discovery of the Accessible Primary Amino Group-Containing Segments from Cell Surface Proteins by Fine-Tuning a High-Throughput Biotinylation Method. Int J Mol Sci. 2022;24(1).
- 67. Lango T, Kuffa K, Tusnady GE. Optimized Biotinylated Peptide Detection Method for Characterizing the Cell Surface Proteome. Methods Mol Biol. 2025;2908:13-31.

- 68. Szebenyi K, Furedi A, Bajtai E, Sama SN, Csiszar A, Gombos B, Szabo P, Grusch M, Szakacs G. Effective targeting of breast cancer by the inhibition of P-glycoprotein mediated removal of toxic lipid peroxidation byproducts from drug tolerant persister cells. Drug Resist Updat. 2023;71:101007.
- 69. Neve RM, Chin K, Fridlyand J, Yeh J, Baehner FL, Fevr T, Clark L, Bayani N, Coppe JP, Tong F, Speed T, Spellman PT, DeVries S, Lapuk A, Wang NJ, Kuo WL, Stilwell JL, Pinkel D, Albertson DG, Waldman FM, McCormick F, Dickson RB, Johnson MD, Lippman M, Ethier S, Gazdar A, Gray JW. A collection of breast cancer cell lines for the study of functionally distinct cancer subtypes. Cancer Cell. 2006;10(6):515-27.
- 70. Javaid S, Schaefer A, Goodwin CM, Nguyen VV, Massey FL, Pierobon M, Gambrell-Sanders D, Waters AM, Lambert KN, Diehl JN, Hobbs GA, Wood KC, Petricoin EF, Der CJ, Cox AD. Concurrent Inhibition of ERK and Farnesyltransferase Suppresses the Growth of HRAS Mutant Head and Neck Squamous Cell Carcinoma. Mol Cancer Ther. 2022;21(5):762-74.
- 71. Roberts AW, Davids MS, Pagel JM, Kahl BS, Puvvada SD, Gerecitano JF, Kipps TJ, Anderson MA, Brown JR, Gressick L, Wong S, Dunbar M, Zhu M, Desai MB, Cerri E, Heitner Enschede S, Humerickhouse RA, Wierda WG, Seymour JF. Targeting BCL2 with Venetoclax in Relapsed Chronic Lymphocytic Leukemia. N Engl J Med. 2016;374(4):311-22.
- 72. Zhan Y, Jiang L, Jin X, Ying S, Wu Z, Wang L, Yu W, Tong J, Zhang L, Lou Y, Qiu Y. Inhibiting RRM2 to enhance the anticancer activity of chemotherapy. Biomed Pharmacother. 2021;133:110996.
- 73. Wang T, Liu P, Yang J. Targeting SAMHD1: To overcome multiple anti-cancer drugs resistance in hematological malignancies. Genes Dis. 2023;10(3):891-900.
- 74. Herold N, Rudd SG, Sanjiv K, Kutzner J, Bladh J, Paulin CBJ, Helleday T, Henter JI, Schaller T. SAMHD1 protects cancer cells from various nucleoside-based antimetabolites. Cell Cycle. 2017;16(11):1029-38.
- 75. Saiki Y, Yoshino Y, Fujimura H, Manabe T, Kudo Y, Shimada M, Mano N, Nakano T, Lee Y, Shimizu S, Oba S, Fujiwara S, Shimizu H, Chen N, Nezhad ZK, Jin G, Fukushige S, Sunamura M, Ishida M, Motoi F, Egawa S, Unno M, Horii A. DCK is frequently inactivated in acquired gemcitabine-resistant human cancer cells. Biochem Biophys Res Commun. 2012;421(1):98-104.

- 76. Swords RT, Coutre S, Maris MB, Zeidner JF, Foran JM, Cruz J, Erba HP, Berdeja JG, Tam W, Vardhanabhuti S, Pawlikowska-Dobler I, Faessel HM, Dash AB, Sedarati F, Dezube BJ, Faller DV, Savona MR. Pevonedistat, a first-in-class NEDD8-activating enzyme inhibitor, combined with azacitidine in patients with AML. Blood. 2018;131(13):1415-24.
- 77. Podar K, Shah J, Chari A, Richardson PG, Jagannath S. Selinexor for the treatment of multiple myeloma. Expert Opin Pharmacother. 2020;21(4):399-408.
- 78. Gjertsen BT, Schoffski P. Discovery and development of the Polo-like kinase inhibitor volasertib in cancer therapy. Leukemia. 2015;29(1):11-9.
- 79. Christman JK. 5-Azacytidine and 5-aza-2'-deoxycytidine as inhibitors of DNA methylation: mechanistic studies and their implications for cancer therapy. Oncogene. 2002;21(35):5483-95.
- 80. Smith SS, Kaplan BE, Sowers LC, Newman EM. Mechanism of human methyldirected DNA methyltransferase and the fidelity of cytosine methylation. Proc Natl Acad Sci U S A. 1992;89(10):4744-8.
- 81. Robey RW, Pluchino KM, Hall MD, Fojo AT, Bates SE, Gottesman MM. Revisiting the role of ABC transporters in multidrug-resistant cancer. Nat Rev Cancer. 2018;18(7):452-64.
- 82. Weber R, Groth C, Lasser S, Arkhypov I, Petrova V, Altevogt P, Utikal J, Umansky V. IL-6 as a major regulator of MDSC activity and possible target for cancer immunotherapy. Cell Immunol. 2021;359:104254.
- 83. Mirlekar B. Tumor promoting roles of IL-10, TGF-beta, IL-4, and IL-35: Its implications in cancer immunotherapy. SAGE Open Med. 2022;10:20503121211069012.
- 84. Shimamura T, Fujisawa T, Husain SR, Joshi B, Puri RK. Interleukin 13 mediates signal transduction through interleukin 13 receptor alpha2 in pancreatic ductal adenocarcinoma: role of IL-13 Pseudomonas exotoxin in pancreatic cancer therapy. Clin Cancer Res. 2010;16(2):577-86.
- 85. Lango T, Rona G, Hunyadi-Gulyas E, Turiak L, Varga J, Dobson L, Varady G, Drahos L, Vertessy BG, Medzihradszky KF, Szakacs G, Tusnady GE. Identification of Extracellular Segments by Mass Spectrometry Improves Topology Prediction of Transmembrane Proteins. Sci Rep. 2017;7:42610.

- 86. Basisty N, Kale A, Jeon OH, Kuehnemann C, Payne T, Rao C, Holtz A, Shah S, Sharma V, Ferrucci L, Campisi J, Schilling B. A proteomic atlas of senescence-associated secretomes for aging biomarker development. PLoS Biol. 2020;18(1):e3000599.
- 87. Zhou L, Zeng Y, Liu Y, Du K, Luo Y, Dai Y, Pan W, Zhang L, Zhang L, Tian F, Gu C. Cellular senescence and metabolic reprogramming model based on bulk/single-cell RNA sequencing reveals PTGER4 as a therapeutic target for ccRCC. BMC Cancer. 2024;24(1):451.
- 88. Wiley CD, Liu S, Limbad C, Zawadzka AM, Beck J, Demaria M, Artwood R, Alimirah F, Lopez-Dominguez JA, Kuehnemann C, Danielson SR, Basisty N, Kasler HG, Oron TR, Desprez PY, Mooney SD, Gibson BW, Schilling B, Campisi J, Kapahi P. SILAC Analysis Reveals Increased Secretion of Hemostasis-Related Factors by Senescent Cells. Cell Rep. 2019;28(13):3329-37 e5.
- 89. Ma Y, Liang Y, Liang N, Zhang Y, Xiao F. Identification and functional analysis of senescence-associated secretory phenotype of premature senescent hepatocytes induced by hexavalent chromium. Ecotoxicol Environ Saf. 2021;211:111908.
- 90. Huang Y, Wang J, Jiang C, Zheng M, Han M, Fang Q, Liu Y, Li R, Zhong L, Li Z. ANXA2 promotes osteogenic differentiation and inhibits cellular senescence of periodontal ligament cells (PDLCs) in high glucose conditions. PeerJ. 2024;12:e18064.
- 91. Sofiadis K, Josipovic N, Nikolic M, Kargapolova Y, Ubelmesser N, Varamogianni-Mamatsi V, Zirkel A, Papadionysiou I, Loughran G, Keane J, Michel A, Gusmao EG, Becker C, Altmuller J, Georgomanolis T, Mizi A, Papantonis A. HMGB1 coordinates SASP-related chromatin folding and RNA homeostasis on the path to senescence. Mol Syst Biol. 2021;17(6):e9760.
- 92. Lu H, Zhang Z, Barnie PA, Su Z. Dual faced HMGB1 plays multiple roles in cardiomyocyte senescence and cardiac inflammatory injury. Cytokine Growth Factor Rev. 2019;47:74-82.
- 93. Conte M, Giuliani C, Chiariello A, Iannuzzi V, Franceschi C, Salvioli S. GDF15, an emerging key player in human aging. Ageing Res Rev. 2022;75:101569.
- 94. Ewald JA, Desotelle JA, Wilding G, Jarrard DF. Therapy-induced senescence in cancer. J Natl Cancer Inst. 2010;102(20):1536-46.
- 95. Ashraf HM, Fernandez B, Spencer SL. The intensities of canonical senescence biomarkers integrate the duration of cell-cycle withdrawal. bioRxiv. 2023.

- 96. Hudgins AD, Tazearslan C, Tare A, Zhu Y, Huffman D, Suh Y. Age- and Tissue-Specific Expression of Senescence Biomarkers in Mice. Front Genet. 2018;9:59.
- 97. Lim HJ, Jang WB, Rethineswaran VK, Choi J, Lee EJ, Park S, Jeong Y, Ha JS, Yun J, Choi YJ, Hong YJ, Kwon SM. StemRegenin-1 Attenuates Endothelial Progenitor Cell Senescence by Regulating the AhR Pathway-Mediated CYP1A1 and ROS Generation. Cells. 2023;12(15).
- 98. Zhao M, Pan B, He Y, Niu B, Gao X. Elucidating the pharmacological mechanism by which Si-Wu-Tang induces cellular senescence in breast cancer via multilevel data integration. Aging (Albany NY). 2022;14(14):5812-37.
- 99. Tesch GH, Ma FY, Ozols E, Nikolic-Paterson DJ. Intervention treatment reducing cellular senescence inhibits tubulointerstitial fibrosis in diabetic mice following acute kidney injury. Clin Sci (Lond). 2024;138(5):309-26.
- 100. Anerillas C, Herman AB, Munk R, Garrido A, Lam KG, Payea MJ, Rossi M, Tsitsipatis D, Martindale JL, Piao Y, Mazan-Mamczarz K, Fan J, Cui CY, De S, Abdelmohsen K, de Cabo R, Gorospe M. A BDNF-TrkB autocrine loop enhances senescent cell viability. Nat Commun. 2022;13(1):6228.
- 101. Prakash S, Agrawal S, Vahed H, Ngyuen M, BenMohamed L, Gupta S, Agrawal A. Dendritic cells from aged subjects contribute to chronic airway inflammation by activating bronchial epithelial cells under steady state. Mucosal Immunol. 2014;7(6):1386-94.
- 102. Nygaard M, Dowsett J, McGue M, Christensen K, Christiansen L, Tan Q, Mengel-From J. Genome-wide association analysis of cognitive function in Danish long-lived individuals. Mech Ageing Dev. 2021;195:111463.
- 103. Niu RZ, Feng WQ, Yu QS, Shi LL, Qin QM, Liu J. Integrated analysis of plasma proteome and cortex single-cell transcriptome reveals the novel biomarkers during cortical aging. Front Aging Neurosci. 2023;15:1063861.
- 104. Doshida Y, Hashimoto S, Iwabuchi S, Takino Y, Ishiwata T, Aigaki T, Ishigami A. Single-cell RNA sequencing to detect age-associated genes that identify senescent cells in the liver of aged mice. Sci Rep. 2023;13(1):14186.
- 105. Chen X, Zhang W, Gao YF, Su XQ, Zhai ZH. Senescence-like changes induced by expression of p21(waf1/Cip1) in NIH3T3 cell line. Cell Res. 2002;12(3-4):229-33.

- 106. Dai CY, Enders GH. p16 INK4a can initiate an autonomous senescence program. Oncogene. 2000;19(13):1613-22.
- 107. Furedi A, Szebenyi K, Toth S, Cserepes M, Hamori L, Nagy V, Karai E, Vajdovich P, Imre T, Szabo P, Szuts D, Tovari J, Szakacs G. Pegylated liposomal formulation of doxorubicin overcomes drug resistance in a genetically engineered mouse model of breast cancer. J Control Release. 2017;261:287-96.
- 108. Rottenberg S, Nygren AO, Pajic M, van Leeuwen FW, van der Heijden I, van de Wetering K, Liu X, de Visser KE, Gilhuijs KG, van Tellingen O, Schouten JP, Jonkers J, Borst P. Selective induction of chemotherapy resistance of mammary tumors in a conditional mouse model for hereditary breast cancer. Proc Natl Acad Sci U S A. 2007;104(29):12117-22.
- 109. Legrier ME, Bieche I, Gaston J, Beurdeley A, Yvonnet V, Deas O, Thuleau A, Chateau-Joubert S, Servely JL, Vacher S, Lassalle M, Depil S, Tucker GC, Fontaine JJ, Poupon MF, Roman-Roman S, Judde JG, Decaudin D, Cairo S, Marangoni E. Activation of IFN/STAT1 signalling predicts response to chemotherapy in oestrogen receptornegative breast cancer. Br J Cancer. 2016;114(2):177-87.
- 110. Weichselbaum RR, Ishwaran H, Yoon T, Nuyten DS, Baker SW, Khodarev N, Su AW, Shaikh AY, Roach P, Kreike B, Roizman B, Bergh J, Pawitan Y, van de Vijver MJ, Minn AJ. An interferon-related gene signature for DNA damage resistance is a predictive marker for chemotherapy and radiation for breast cancer. Proc Natl Acad Sci U S A. 2008;105(47):18490-5.
- 111. Li MF, Zhang DH, Wang LS, Yue CF, Pang LJ, Guo YM, Yang ZG. Construction and validation of a SASP-related prognostic signature in patients with acute myeloid leukaemia. J Cell Mol Med. 2024;28(16):e70017.
- 112. Pidugu VK, Wu MM, Yen AH, Pidugu HB, Chang KW, Liu CJ, Lee TC. IFIT1 and IFIT3 promote oral squamous cell carcinoma metastasis and contribute to the antitumor effect of gefitinib via enhancing p-EGFR recycling. Oncogene. 2019;38(17):3232-47.
- 113. Wang X, Qian H, Yang L, Yan S, Wang H, Li X, Yang D. The role and mechanism of IFITM1 in developing acquired cisplatin resistance in small cell lung cancer. Heliyon. 2024;10(10):e30806.

- 114. Sun S, Yoon JS, Kim YS, Won HS. P53 Status Influences the Anti-proliferative Effect Induced by IFITM1 Inhibition in Estrogen Receptor-positive Breast Cancer Cells. Cancer Genomics Proteomics. 2024;21(5):511-22.
- 115. Samaraweera L, Adomako A, Rodriguez-Gabin A, McDaid HM. A Novel Indication for Panobinostat as a Senolytic Drug in NSCLC and HNSCC. Sci Rep. 2017;7(1):1900.
- 116. Gong P, Wang Y, Jing Y. Apoptosis Induction by Histone Deacetylase Inhibitors in Cancer Cells: Role of Ku70. Int J Mol Sci. 2019;20(7).
- 117. Wojcik C. Regulation of apoptosis by the ubiquitin and proteasome pathway. J Cell Mol Med. 2002;6(1):25-48.
- 118. Nishihara S, Yamaoka T, Ishikawa F, Higuchi K, Hasebe Y, Manabe R, Kishino Y, Kusumoto S, Ando K, Kuroda Y, Ohmori T, Sagara H, Yoshida H, Tsurutani J. Mechanisms of EGFR-TKI-Induced Apoptosis and Strategies Targeting Apoptosis in EGFR-Mutated Non-Small Cell Lung Cancer. Genes (Basel). 2022;13(12).
- 119. Moore N, Houghton J, Lyle S. Slow-cycling therapy-resistant cancer cells. Stem Cells Dev. 2012;21(10):1822-30.
- 120. Ding L, Cao J, Lin W, Chen H, Xiong X, Ao H, Yu M, Lin J, Cui Q. The Roles of Cyclin-Dependent Kinases in Cell-Cycle Progression and Therapeutic Strategies in Human Breast Cancer. Int J Mol Sci. 2020;21(6).
- 121. Morande PE, Sivina M, Uriepero A, Seija N, Berca C, Fresia P, Landoni AI, Di Noia JM, Burger JA, Oppezzo P. Ibrutinib therapy downregulates AID enzyme and proliferative fractions in chronic lymphocytic leukemia. Blood. 2019;133(19):2056-68.
- 122. Metibemu DS, Akinloye OA, Akamo AJ, Ojo DA, Okeowo OT, Omotuyi IO. Exploring receptor tyrosine kinases-inhibitors in Cancer treatments. Egyptian Journal of Medical Human Genetics. 2019;20(1):35.
- 123. Ertel M, Brunhilda T, Panesso S, Sannino S, Sagan A, McGonigal S, Jiang Q, Brodsky J, Osmanbeyoglu H, Buckanovich R. Quiescence as a therapeutic target in ovarian cancer (1245). Gynecologic Oncology. 2023;176:S155-S6.
- 124. Lindqvist LM, Vikstrom I, Chambers JM, McArthur K, Ann Anderson M, Henley KJ, Happo L, Cluse L, Johnstone RW, Roberts AW, Kile BT, Croker BA, Burns CJ, Rizzacasa MA, Strasser A, Huang DC. Translation inhibitors induce cell death by

- multiple mechanisms and Mcl-1 reduction is only a minor contributor. Cell Death Dis. 2012;3(10):e409.
- 125. Thirumaran R, Prendergast GC, Gilman PB. Chapter 7 Cytotoxic Chemotherapy in Clinical Treatment of Cancer. In: Prendergast GC, Jaffee EM, editors. Cancer Immunotherapy. Burlington: Academic Press; 2007. p. 101-16.
- 126. Pu Y, Li L, Peng H, Liu L, Heymann D, Robert C, Vallette F, Shen S. Drugtolerant persister cells in cancer: the cutting edges and future directions. Nat Rev Clin Oncol. 2023;20(11):799-813.
- 127. Deschenes M, Chabot B. The emerging role of alternative splicing in senescence and aging. Aging Cell. 2017;16(5):918-33.
- 128. Kwon SM, Min S, Jeoun UW, Sim MS, Jung GH, Hong SM, Jee BA, Woo HG, Lee C, Yoon G. Global spliceosome activity regulates entry into cellular senescence. FASEB J. 2021;35(1):e21204.
- 129. Georgilis A, Klotz S, Hanley CJ, Herranz N, Weirich B, Morancho B, Leote AC, D'Artista L, Gallage S, Seehawer M, Carroll T, Dharmalingam G, Wee KB, Mellone M, Pombo J, Heide D, Guccione E, Arribas J, Barbosa-Morais NL, Heikenwalder M, Thomas GJ, Zender L, Gil J. PTBP1-Mediated Alternative Splicing Regulates the Inflammatory Secretome and the Pro-tumorigenic Effects of Senescent Cells. Cancer Cell. 2018;34(1):85-102 e9.
- 130. Ivanova OM, Anufrieva KS, Kazakova AN, Malyants IK, Shnaider PV, Lukina MM, Shender VO. Non-canonical functions of spliceosome components in cancer progression. Cell Death Dis. 2023;14(2):77.
- 131. Marin I, Boix O, Garcia-Garijo A, Sirois I, Caballe A, Zarzuela E, Ruano I, Attolini CS, Prats N, Lopez-Dominguez JA, Kovatcheva M, Garralda E, Munoz J, Caron E, Abad M, Gros A, Pietrocola F, Serrano M. Cellular Senescence Is Immunogenic and Promotes Antitumor Immunity. Cancer Discov. 2023;13(2):410-31.
- 132. Prata L, Ovsyannikova IG, Tchkonia T, Kirkland JL. Senescent cell clearance by the immune system: Emerging therapeutic opportunities. Semin Immunol. 2018;40:101275.
- 133. Wang TW, Johmura Y, Suzuki N, Omori S, Migita T, Yamaguchi K, Hatakeyama S, Yamazaki S, Shimizu E, Imoto S, Furukawa Y, Yoshimura A, Nakanishi M. Blocking

- PD-L1-PD-1 improves senescence surveillance and ageing phenotypes. Nature. 2022;611(7935):358-64.
- 134. Pereira BI, Devine OP, Vukmanovic-Stejic M, Chambers ES, Subramanian P, Patel N, Virasami A, Sebire NJ, Kinsler V, Valdovinos A, LeSaux CJ, Passos JF, Antoniou A, Rustin MHA, Campisi J, Akbar AN. Senescent cells evade immune clearance via HLA-E-mediated NK and CD8(+) T cell inhibition. Nat Commun. 2019;10(1):2387.
- 135. Lv Y, Ma X, Ma Y, Du Y, Feng J. A new emerging target in cancer immunotherapy: Galectin-9 (LGALS9). Genes Dis. 2023;10(6):2366-82.
- 136. Choi YW, Kim YH, Oh SY, Suh KW, Kim YS, Lee GY, Yoon JE, Park SS, Lee YK, Park YJ, Kim HS, Park SH, Kim JH, Park TJ. Senescent Tumor Cells Build a Cytokine Shield in Colorectal Cancer. Adv Sci (Weinh). 2021;8(4):2002497.
- 137. Ajith A, Mamouni K, Horuzsko DD, Musa A, Dzutsev AK, Fang JR, Chadli A, Zhu X, Lebedyeva I, Trinchieri G, Horuzsko A. Targeting TREM1 augments antitumor T cell immunity by inhibiting myeloid-derived suppressor cells and restraining anti-PD-1 resistance. J Clin Invest. 2023;133(21).
- 138. Torke S, Walther W, Stein U. Immune Response and Metastasis-Links between the Metastasis Driver MACC1 and Cancer Immune Escape Strategies. Cancers (Basel). 2024;16(7).

# 9. Bibliography of the candidate's publications

## This PhD thesis is based on the following publications:

**Bajtai** E, Kiss C, Bakos É, Langó T, Lovrics A, Schád É, Tisza V, Hegedűs K, Fürjes P, Szabó Z, Tusnády GE, Szakács G, Tantos Á, Spisák S, Tóvári J, Füredi A. Therapyinduced senescence is a transient drug resistance mechanism in breast cancer. Mol Cancer. 2025 May 1;24(1):128. doi: 10.1186/s12943-025-02310-0. PMID: 40312750; PMCID: PMC12044945. **IF: 33.9** 

Szebényi K, Füredi A, **Bajtai E**, Sama SN, Csiszar A, Gombos B, Szabó P, Grusch M, Szakács G. Effective targeting of breast cancer by the inhibition of P-glycoprotein mediated removal of toxic lipid peroxidation byproducts from drug tolerant persister cells. Drug Resist Updat. 2023 Nov;71:101007. doi: 10.1016/j.drup.2023.101007. Epub 2023 Sep 17. PMID: 37741091. **IF: 21.7** 

### Other publications:

Füredi A, Tóth S, Hegedüs K, Szabó PT, Gaál A, Barta G, Naszályi LN, Kiss K, Bölcskei K, Szeltner Z, **Bajtai E**, Gombos B, Kiss D, Cserepes MT, Kiss A, Pokreisz P, Kenner L, Högler S, Magyar C, Cowles JD, Csiszar A, Tóvári J, Szüts D, Helyes Z, Varga Z, Mező G, Szakács G. Safe delivery of a highly toxic anthracycline derivative through liposomal nanoformulation achieves complete cancer regression. Mol Cancer. 2025. Accepted for publication. Ref: Submission ID 11580c0e-613a-4161-963b-348f39e47065. **IF: 33.9** 

Vizvari Z, Gyorfi N, Maczko G, Varga R, Jakabfi-Csepregi R, Sari Z, Furedi A, **Bajtai** E, Vajda F, Tadic V, Odry P, Karadi Z, Toth A. Reproducibility analysis of bioimpedance-based self-developed live cell assays. Sci Rep. 2024 Jul 16;14(1):16380. doi: 10.1038/s41598-024-67061-2. PMID: 39013939; PMCID: PMC11252348. **IF:3.9** 

Vajda F, **Bajtai** E, Gombos B, Karai E, Hámori L, Szakács G, Füredi A. Új stratégiák fejlesztése a gyógyszerrezisztens daganatok kezeléséhez [Development of novel treatment strategies for drug resistant cancer]. Magy Onkol. 2021 Jun 3;65(2):176-187. Hungarian. Epub 2021 May 9. PMID: 34081765.

# 10. Acknowledgements

I would like to express my sincere gratitude to my supervisors, András Füredi and József Tóvári, for their continuous support, guidance and advice throughout my doctoral studies, as well as for their dedicated mentorship.

I'm also grateful to Gergő Szakács, head of the Drug Resistance Research Group for his support during my work. I thank my colleagues in the group – Éva Bakos, Flóra Vajda, Szilárd Tóth, Balázs Gombos, Anna Lovrics, Dániel Kiss and Krisztina Dolniczki – for all their help, teamwork, and support along the way. Special thanks to Krisztina Mohos for her constant help, support with order management, and for always being there as a friend. I am especially grateful to Kornélia Szebényi, whose findings were essential to the foundation of this project.

I would also like to thank the Department of Experimental Pharmacology at the National Institute of Oncology, especially Hidvégi Anita and Lénárt Violetta, for teaching me and supporting me with the animal experiments.

I'm thankful to all my co-authors – Csaba Kiss, Éva Bakos, Tamás Langó, Anna Lovrics, Éva Schád, Viktória Tisza, Károly Hegedűs, Péter Fürjes, Zoltán Szabó, Gábor E. Tusnády, Gergely Szakács, Ágnes Tantos, Sándor Spisák, József Tóvári, and András Füredi – for their contributions and collaborative efforts, which were essential to my first-author publication.

Finally, I would like to thank my friends and my family for their continuous support, patience, and understanding throughout the years. I am especially grateful to my mother and my grandmother, whose love, strength, and unwavering support have always been there for me – I know that they will be the proudest of all.